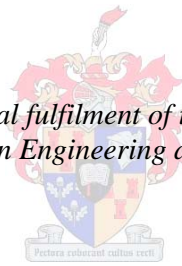


Phase Noise Measurement

by
Johannes Jacobus Grobbelaar

*Thesis presented in partial fulfilment of the requirements for the degree
Master of Science in Engineering at Stellenbosch University*



Supervisor: Prof J.B. de Swardt
Department of Electrical and Electronic Engineering

March 2011

Declaration

By submitting this dissertation electronically, I declare that the entirety of the work contained therein is my own, original work, that I am the sole author thereof (save to the extent explicitly otherwise stated), that reproduction and publication thereof by Stellenbosch University will not infringe any third party rights and that I have not previously in its entirety or in part submitted it for obtaining any qualification.

Date: March 2011

Copyright ©

2011 Stellenbosch University. All rights reserved.

Declaration

By submitting this thesis electronically, I declare that the entirety of the work contained therein is my own, original work, that I am the sole author thereof (save to the extent explicitly otherwise stated), that reproduction and publication thereof by Stellenbosch University will not infringe any third party rights and that I have not previously in its entirety or in part submitted it for obtaining any qualification.

Date:

Copyright © 2011 Stellenbosch University
All rights reserved.

Abstract

Keywords - phase noise measurement, crosscorrelation, averaging, phase demodulation

The objective of the thesis is the development of a phase noise measuring system that makes use of crosscorrelation and averaging to measure below the system hardware noise floor.

Various phase noise measurement techniques are considered after which the phase demodulation method is chosen to be implemented. The full development cycle of the hardware is discussed, as well as the post processing that is performed on the measured phase noise.

Uittreksel

Sleutelwoorde - faseruis meting, kruiskorrelasie, vergemiddeling, fase demodulasie

Die doel van hierdie tesis is die ontwikkeling van 'n faseruis meetstelsel wat gebruik maak van kruiskorrelasie en vergemiddeling om onder die ruisvloer van die meetstelsel se hardeware te meet.

Verskeie faseruis meettegnieke word ondersoek en die fase demodulasie metode word gekies om geïmplementeer te word. Die volle ontwikkelingsiklus van die hardeware word bespreek, sowel as die naverwerking wat toegepas is op die gemete faseruis.

Acknowledgments

My sincerest gratitude to everyone who contributed to this thesis.

I would like to thank my supervisor, Prof J.B. de Swardt, for his continual support, guidance and encouragement throughout the thesis.

Many thanks to Prof P.W. van der Walt, for his technical insights.

Much gratitude to Reutech Radar System for their financial aid, without which this project would not have been possible.

To my friends, Jonathan Hoole and JP Taylor, for the millions of questions they answered.

Thank you to my parents for their support and interest in my work.

The most thanks goes to my fiancé, Wilmarie Hagan, for her continual support and encouragement. Thank you for all the lunches that you made. The path to a man's heart apparently is through his *low noise* stomach.

Dedication

To my fiancée...

Contents

Declaration	i
Abstract	ii
Uittreksel	iii
Acknowledgments	iv
Dedication	v
Contents	vi
List of Figures	x
List of Tables	xiii
List of Abbreviations	xiv
List of Symbols	xvi
1 Introduction	1
1.1 Problem Statement	1
1.2 Proposed Solution	1
1.3 Overview of Thesis	2
2 Introductory Phase Noise Theory	3
2.1 Introduction	3
2.2 Frequency, Phase and Amplitude Noise	3
2.3 Amplitude Noise	5
2.4 Phase Noise	7

2.5	Phasor Representation of Amplitude & Phase Noise	9
2.6	Characterization of Frequency, Amplitude and Phase Instabilities	10
2.6.1	Amplitude noise	10
2.6.2	Frequency noise	11
2.6.3	Phase noise	12
2.7	Conclusion	13
3	Phase Noise Measurement Methods	15
3.1	Introduction	15
3.2	Normalized Frequency Difference	15
3.3	Phase Noise Measuring Techniques	16
3.3.1	Spectrum analyzer measurement	16
3.3.2	Heterodyne (beat frequency) method	17
3.3.3	Time difference method	18
3.3.4	Dual mixer time difference system	19
3.3.5	Frequency demodulation	21
3.3.6	Phase demodulation	22
3.4	Conclusion	24
4	Hardware	25
4.1	Introduction	25
4.2	Hardware Design Specifications	25
4.3	PLL	27
4.3.1	Introduction	27
4.3.2	Components	28
4.3.3	PLL Bandwidth	34
4.3.4	Complete circuit model	35
4.3.5	Simulation of PLL	36
4.3.6	Measurement of PLL bandwidth	37
4.3.7	Conclusion	38
4.4	LNA Prefilter	38
4.4.1	Introduction	38
4.4.2	LNA Prefilter design & simulation	39
4.4.3	Measurement	41
4.4.4	Conclusion	42
4.5	LNA	42
4.5.1	Introduction	42
4.5.2	LNA Design	42

4.5.3	Simulation	44
4.5.4	Measurement	46
4.5.5	Conclusion	47
4.6	LNA Output LPF	47
4.7	ADC Prefilters	48
4.7.1	Introduction	48
4.7.2	ADC Prefilters Design & Simulation	49
4.7.3	Measurements	51
4.7.4	Conclusion	52
4.8	Conclusion	52
5	Data Acquisition & Digital Signal Processing	53
5.1	Introduction	53
5.2	ADC - Tektronix TDS 1002B	53
5.3	FFT Analysis of ADC output	54
5.3.1	Test Setup for FFT analysis of ADC output	54
5.3.2	FFT Noise Floor	56
5.4	Conclusion	57
6	Calibration of Measuring System	58
6.1	Introduction	58
6.2	Gain linearity	58
6.3	Phase Noise Measurement Calibration	60
6.3.1	Angle Modulation Theory	60
6.3.2	Phase Noise Measurement Calibration	61
6.4	Dynamic Range	64
6.4.1	Introduction	64
6.4.2	Maximum phase noise measurable	65
6.4.3	Minimum phase noise measurable	65
6.4.4	Conclusion	67
6.5	Conclusion	68
7	Crosscorrelation and Averaging	69
7.1	Introduction	69
7.2	Correlation Theory	69
7.3	Correlation Simulations	70
7.3.1	Introduction	70
7.3.2	Simulation 1 - Lowering the noise floor	70

7.3.3	Simulation 2 - Improvement in noise floor with relation to number of averages	73
7.3.4	Conclusion	73
7.4	Correlation Measurements	74
7.4.1	Introduction	74
7.4.2	Measurement 1 - Crosscorrelation phase noise measurement	74
7.4.3	Measurement 2 - Voltage spectral density crosscorrelation measurement	76
7.4.4	Conclusion	79
7.5	Limits to Crosscorrelation and averaging	80
7.6	Conclusion	80
8	Conclusion	81
8.1	General Conclusion	81
8.2	Recommendations	81
	Bibliography	82
A	Appendix A	A-1
A.1	PCB layout & EMI shielding	A-1

List of Figures

2.1	Sinusoid containing both AM and PM noise, generated in Matlab	4
2.2	Sinusoid with amplitude noise	5
2.3	Different forms by which amplitude noise is presented.	6
2.4	Phase noise contaminated sinusoid.	7
2.5	Different forms by which phase noise is presented	9
2.6	Phasor representation of a sinusoid with amplitude- and phase noise	10
2.7	Frequency domain representations of phase noise.	13
3.1	Spectrum analyzer phase noise measurement setup	17
3.2	Heterodyne (beat frequency) measurement setup	18
3.3	Time difference method	19
3.4	Duel mixer time difference method	20
3.5	Frequency demodulation phase noise measurement method	21
3.6	Phase demodulation phase noise measurement method	24
4.1	Adapted phase demodulation method with hardware design specifications.	26
4.2	Phase Locked Loop feedback system	27
4.3	PLL with substituted parameters.	28
4.4	Typical model of a mixer	29
4.5	Two 10 MHz VCXO signals are mixed and filtered, resulting in the difference frequencies $K_p \cos(\phi_1 - \phi_2)$	30
4.6	LT Spice simulation results illustrating the different mixer gains K_p for the two cases of series inductor first or parallel capacitor first at the output of the mixer.	31
4.7	VCO sensitivity curve for the leaded 10 MHz VCXO from IQD Frequency Products	32
4.8	Type 2 second order root locus of $G(s)H(s) = \frac{(s+a)K}{s^2}$	33
4.9	Active PLL filter design	34
4.10	Laplace representation of PLL with substituted values for figure 4.3.	35

4.11	PLL open loop simulation bode plot	36
4.12	Phase locked loop closed loop simulation bode plot	37
4.13	Measuring the PLL bandwidth	38
4.14	PLL closed loop amplitude response	38
4.15	Normalized $1\ \Omega$, $1\ Hz$ fifth order single loaded Butter-worth LPF	39
4.16	$1\ MHz$, $50\ \Omega$ fifth order single loaded Butter worth passive LPF	40
4.17	Simulated (in LT Spice) amplitude response for a $1\ MHz$, $50\ \Omega$ fifth order single loaded passive Butter worth LPF	41
4.18	Measured amplitude response for the $1\ MHz$, $50\ \Omega$ fifth order single ended passive Butter worth LPF	41
4.19	LNA circuit diagram	43
4.20	ADA4899-1 Small signal frequency response for various gains	43
4.21	LT Spice AC sweep simulation result for <i>Amp 1</i> in figure	45
4.22	LNA LT Spice AC sweep simulation results, measured at the output of <i>Amp 3</i>	46
4.23	Measurement setup for the LNA frequency amplitude response	46
4.24	LNA amplitude response measurement.	47
4.25	ADC Prefilters	49
4.26	ADC Prefilters circuit diagram	50
4.27	LT Spice simulation of ADC Prefilters bandwidths	51
4.28	ADC Prefilter amplitude response measurement	51
5.1	Tektronix TDS 1002B Digital Storage Oscilloscope	54
5.2	Test Setup for FFT Analysis of ADC Output	54
5.3	Square, Hanning and ChebyChev windows are individually applied to a sampled signal that is composed out of a $1V_{rms}\ 300Hz$ component, a $2mV_{rms}\ 350Hz$ component and white noise.	55
5.4	FFT Output for an 8-Bit ADC, Input = $100kHz$, $f_s = 5kSPS$, Average of 5 FFTs, $M = 2500$	56
5.5	FFT Narrow band Spectrum Analyzer	57
6.1	Amplitude linearity measurement setup	59
6.2	Carrier and significant sidebands of a tone modulated signal where $\beta = 1$	61
6.3	Phase noise measurement calibration setup performed by simulating phase noise with a narrow band FM modulated signal.	62
6.4	Phase noise simulation measurement of $J_1(0.25)$ where $f_m = 976.3\ Hz$	63
6.5	Measured values of $J_1(0.25)$ where f_m is swept over $40\ Hz$ to $400\ kHz$	63

6.6	A calibrated phase noise measurement taken by the phase noise measuring system developed in this thesis is compared to a measurement that is taken by a Rohde & Schwartz FSEA30 phase noise measuring instrument.	64
6.7	Noise floor of the phase noise measuring system hardware	67
7.1	The individual noise from each system is added to the composite signal at the input to form $x(t)$ and $y(t)$	71
7.2	The difference between correlation with averaging and only averaging.	72
7.3	Improvement in noise floor when an average of more correlations are performed.	73
7.4	Crosscorrelation phase noise measuring system	75
7.5	Average of 100 crosscorrelations of $J_1(0.25)$ where $f_m = 800 Hz$	75
7.6	Power Spectral Density crosscorrelation measurement setup	76
7.7	Band 1 voltage spectral densities of the thermal noise voltage generated by resistors of size 220Ω , 100Ω , 47Ω , 22Ω , 10Ω and 5.6Ω	77
7.8	Band 2 voltage spectral densities of the thermal noise voltage generated by resistors of size 220Ω , 100Ω , 47Ω , 22Ω , 10Ω and 5.6Ω	78
7.9	Band 3 voltage spectral densities of the thermal noise voltage generated by resistors of size 220Ω , 100Ω , 47Ω , 22Ω , 10Ω and 5.6Ω	79
A.1	Full circuit diagram of the Phase Noise Measuring System	A-2
A.2	PCB layouts	A-3

List of Tables

4.1	Steady state phase errors θ_e for various system types	33
4.2	Different -3 dB cutoff frequencies of the LNA depending on how many of the amplifier stages are included.	45
4.3	ADC Prefilter bands	48
4.4	ADC Prefilter Bandwidths	49
4.5	ADC Prefilter bandwidth and gain measurements	52
6.1	Amplitude linearity measurement results for Band 1	59
6.2	The different gains for each of the Bands, depending on what the gain of the LNA is.	60
6.3	Maximum phase noise measurable in Band 1, Band 2 and Band 3	65
6.4	Minimum phase noise measurable in each of the three Bands, due to the FFT noise floor	66
6.5	Dynamic range for Band 1, 2 and 3	68
7.1	Theoretical dynamic range of Band 1, 2 and 3 when crosscorrelation and averaging is used.	80

List of Abbreviations

AC	Alternating Current
ADC	Analog to Digital Converter
AM	Amplitude Modulation
DC	Direct Current
DMTD	Dual Mixer Time Difference
DSB	Double-Sideband
DUT	Device Under Test
C.E.	Characteristic Equation
FFT	Fast Fourier Transform
FM	Frequency Modulation
HPF	High Pass Filter
IF	Intermediate Frequency
LNA	Low Noise Amplifier
LPF	Low Pass Filter
PDS	Power Density Spectrum
PM	Phase Modulation
RMS	Root Mean Square
RO	Reference Oscillator

SSB	Single-Sideband
SNR	Signal to Noise Ration
SQNR	Signal to Quantization Noise Ratio
VCO	Voltage Controlled Oscillator
VCXO	Voltage Controlled Crystal Oscillator

List of Symbols

Constants:

$$\pi = 3.1415926535897932384626433832795$$

$$e = 2.7182818284590452353602874713526$$

Chapter 1

Introduction

The noise produced by signal sources such as voltage controlled oscillators (VCO's), oscillators or frequency synthesizers is critically important because it may severely degrade the performance of a system such as a wireless system. In addition to adding to the noise level of the receiver, a noisy local oscillator will severely limit how close adjacent channels can be by leading to down-conversion of undesired signals[1].

The short-term random fluctuations in the frequency (or phase) of signal sources are more commonly referred to as phase noise. Phase noise has been singled out to be the dominant bandwidth limiting factor in wireless systems. The need to measure the phase noise generated by oscillators arises from a desire to know how much the oscillator's phase noise is.

1.1 Problem Statement

In order to measure phase noise that is generated by oscillators special equipment is needed. Equipment that can measure phase noise is currently commercially available, but at great financial cost, rendering it unaffordable by many smaller institutes or companies.

1.2 Proposed Solution

This project explores different phase noise measuring techniques and attempts to develop a phase noise measuring system that is competitive with commercially available systems. Crosscorrelation and averaging is employed in an effort to measure below the noise floor of the developed hardware.

1.3 Overview of Thesis

An understanding of phase noise is essential in order to design a phase noise measuring system. Chapter 2 introduces the basic concepts of phase noise with mathematical models and visual time domain representations. Phase noise is then quantified in terms of power spectral density. Other forms of noise that can be mistaken for phase noise, such as amplitude noise, are also discussed in this chapter.

The various existing phase noise measuring methods considered for implementation are evaluated according to their feasibility in Chapter 3. The characteristics of the phase demodulation method are found to be most favorable and is thus chosen as the measuring method of choice.

In Chapter 4 a modular approach is taken in designing the hardware when implementing the phase demodulation method. This approach grants the design some flexibility so that individual hardware components are interchangeable.

The process by which the measured analog phase noise is converted to digital format is discussed in Chapter 5. Post processing of the phase noise follows.

The hardware, data acquisition and digital signal processing combines to form the phase noise measuring system. The calibration of the measuring system is then explained in Chapter 6.

Finally the designed phase noise measuring system is improved by incorporating crosscorrelation and averaging techniques in Chapter 7.

Chapter 2

Introductory Phase Noise Theory

2.1 Introduction

In order to design a measuring system that is capable of measuring phase noise an understanding of phase noise is needed first. This chapter covers the basic concepts of phase noise with mathematical models and visual time domain representations. Phase noise is then quantified in terms of power spectral density.

It is shown that amplitude noise can be misinterpreted for phase noise since both forms of noise cause similar sidebands. Defining both amplitude noise and phase noise mathematically reveals their spectral similarity. Frequency noise and phase noise are shown to be closely related to each other by an integral. The relation between phase noise and frequency noise warrants the need to quantify frequency noise.

2.2 Frequency, Phase and Amplitude Noise

Figure 2.1 shows two signals, one is a noiseless sinusoid and the other is a sinusoid that is contaminated with noise. The noise of the contaminated sinusoid in figure 2.1 is composed of amplitude noise (vertical axis) and phase/frequency noise (horizontal axis). It is not always possible to tell the difference in noise type just by inspection since phase noise can look like amplitude noise and *vi ca versa*. In this case both amplitude and phase noise are known to be present as the signals in figure 2.1 are generated mathematically. The formal definition, presented in equation 2.1, represents a sinusoid along with its amplitude and phase noise components [2, 3, 4].

$$v_0(t) = [V_0 + A(t)] \cos[\omega_0 t + \phi(t)] \quad (2.1)$$

where

- V_0 - desired peak amplitude (in volts)
- $A(t)$ - time varying amplitude instability; the amplitude noise (in volts)
- ω_0 - frequency of the desired signal (in radians per second)
- t - time (in seconds)
- $\phi(t)$ - time varying phase instability; the phase noise (in radians).

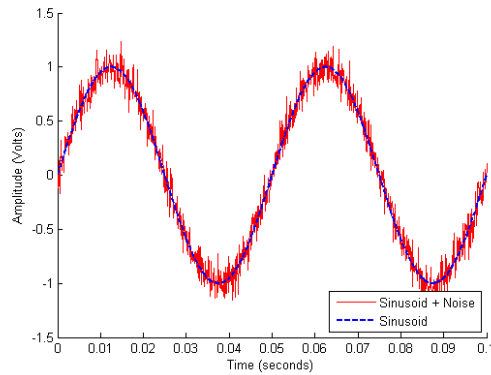


Figure 2.1: Sinusoid containing both AM and PM noise, generated in Matlab

In equation 2.1 amplitude noise is represented by $A(t)$ while phase and frequency noise is represented by $\phi(t)$. Since these instabilities are what corrupts the signal $v_0(t)$, they are considered to be noise and are treated as such in this thesis. Some sources normalize these instabilities [4], as has been done in the following section. The normalized instabilities presented here are all scalar values and represent a ratio of the noise to the nominal.

Amplitude noise is defined in terms of the instantaneous, normalized amplitude deviation as follows [4]

$$a(t) = \frac{A(t)}{V_0}. \quad (2.2)$$

The amplitude noise is normalized to the desired peak amplitude V_0 .

Frequency noise is defined in terms of the instantaneous, normalized frequency deviation $y(t)$ as follows [4]

$$y(t) = \frac{f(t)}{\omega_0} \quad (2.3)$$

where $f(t) = \frac{d}{dt}\phi(t)$. The frequency noise is normalized to the desired frequency ω_0 .

Phase noise is defined in terms of the instantaneous, normalized phase deviation $\phi(t)$ as follows [4]

$$x(t) = \frac{\phi(t)}{\omega_0}. \quad (2.4)$$

The phase noise is also normalized to the desired frequency ω_0 . Note that the instantaneous normalized frequency noise, $y(t)$, is the derivative of the instantaneous normalized phase noise, $x(t)$:

$$y(t) = \frac{d}{dt}x(t). \quad (2.5)$$

2.3 Amplitude Noise

Figure 2.2 shows a comparison between a noiseless sinusoid and one containing amplitude noise. In both plots the peak amplitude V_0 is taken at unity ($V_0 = 1V$). The amplitude noise containing sinusoid crosses the zero amplitude level at regular intervals and is perfectly in phase with the noiseless signal. This is a special case where the phase noise $\phi(t)$ in equation 2.1 is zero. Figure 2.2 shows the special case (solid-line plot) where the amplitude noise $A(t)$ is a sinusoid by letting

$$A(t) = \alpha \cos(\omega_m t) \quad (2.6)$$

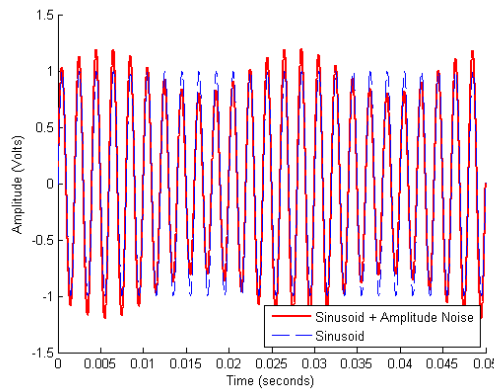


Figure 2.2: Sinusoid with amplitude noise

where $f_m = \omega_m/2\pi$ is the amplitude modulation (AM) frequency and α is the peak amplitude deviation (also called the amplitude modulation index). A sinusoidal shape originates around the maximum ($V_0 = +1V$) and minimum ($V_0 = -1V$) amplitudes. This sinusoidal shape is the sinusoidal amplitude noise defined in equation 2.6 at the maximum amplitude. At the minimum amplitude it is $-A(t)$ with the minus sign signifying a 180° shift in phase. Substituting equation 2.6 into equation 2.1 gives

$$\begin{aligned} v_{AM} &= [1 + \alpha \cos(\omega_m t)] \cos(\omega_0 t) \\ &= \cos(\omega_0 t) + \alpha \cos(\omega_m t) \cos(\omega_0 t) \\ &= \cos(\omega_0 t) + \frac{\alpha}{2} [\cos(\omega_0 + \omega_m) + \cos(\omega_0 - \omega_m)] \end{aligned} \tag{2.7}$$

where $\phi(t) = 0$ for zero phase noise. When viewed in the frequency domain this expression reveals that amplitude noise $A(t)$ in equation 2.6 result in frequency components at $\omega_0 \pm \omega_m$, which are located on either side of the carrier ω_0 . Amplitude noise $A(t)$ can be either discrete or random in nature. Discrete amplitude noise means that the amplitude modulation frequency ω_m is constant and would appear in the frequency spectrum as seen in figure 2.3(a). When the amplitude modulation frequency ω_m is random, a broad continuous distribution localized about the center frequency ω_0 is formed, as seen in figure 2.3(b).

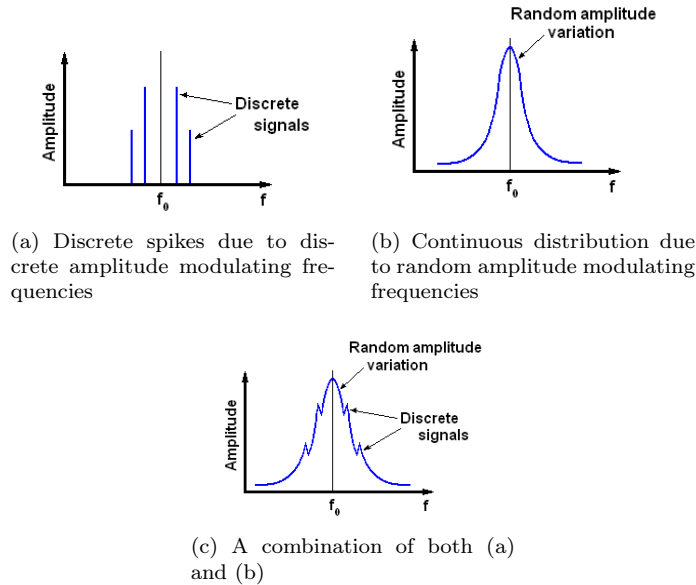


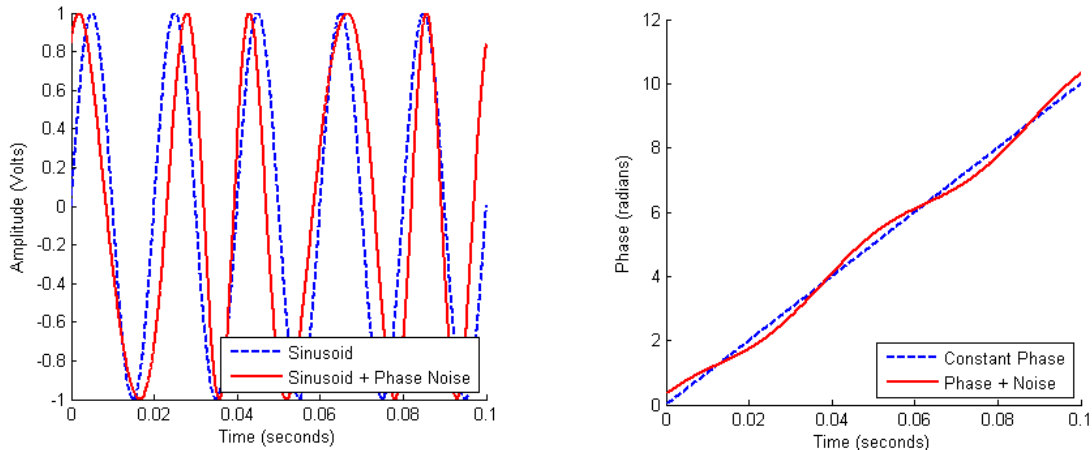
Figure 2.3: Different forms by which amplitude noise is presented.

2.4 Phase Noise

A time domain example of a signal with phase noise is shown in figure 2.4. It is clear from the figure that the amplitude noise component $A(t)$ is zero, since the maximum amplitude of the signal remains at a constant value of $1V$. According to equation 2.1 this leaves $\phi(t)$ as the only source of noise. For illustrative purposes it is assumed that the frequency modulation (FM) frequency would be higher than that of the carrier. The signal without phase noise (dashed-line) goes through zero on the amplitude axis at regular intervals in (a). The corresponding phase increase over time in (b) for this sinusoid is constant (also plotted with a dashed line), which signifies a constant frequency. In contrast, the solid-line plot in (a) crosses the zero amplitude axis at irregular intervals. This results in a non-constant increase in phase shown by the solid-line plot in (b). Frequency is the gradient of the line in (b); therefore the instantaneous frequency is not constant. This illustrates the fact that instantaneous phase variation is indistinguishable from a variation in frequency [2].

Figure 2.4 shows the special case where the phase noise $\phi(t)$ in equation 2.1 is a sinusoid by letting

$$\phi(t) = \frac{\Delta f}{f_m} \sin \omega_m t = \theta_p \sin \omega_m t \quad (2.8)$$



(a) Time domain illustration of a pure sinusoid along with a phase noise contaminated sinusoid.

(b) Constant phase increase over time for the pure sinusoid along with a varying phase increase over time for the phase noise contaminated sinusoid.

Figure 2.4: Phase noise contaminated sinusoid.

where $f_m = \omega_m/2\pi$ is the modulation frequency. The peak phase deviation is $\theta_p = \frac{\Delta f}{f_m}$ (also called the frequency modulation index). A sinusoidal shape in the phase increase over time is noted from figure 2.4(b). Substituting equation 2.8 into equation 2.1 gives

$$v_{PM}(t) = V_0[\cos \omega_0 t \cos(\theta_p \sin \omega_m t) - \sin \omega_0 t \sin(\theta_p \sin \omega_m t)] \quad (2.9)$$

where $A(t) = 0$ for the special case of zero amplitude noise. Assuming the peak phase deviation is small so that $\theta_p \ll 1$, the approximation for small angles can be used, so that $\sin x \cong x$ and $\cos x \cong 1$, simplifying equation 2.9 to

$$\begin{aligned} v_{PM}(t) &= V_0[\cos \omega_0 t - \theta_p \sin \omega_m t \sin \omega_0 t] \\ &= V_0\left\{\cos \omega_0 t - \frac{\theta_p}{2}[\cos(\omega_0 + \omega_m)t - \cos(\omega_0 - \omega_m)t]\right\} \end{aligned} \quad (2.10)$$

This expression shows that small phase deviations $\phi(t)$ in equation 2.1 result in modulation sidebands at $\omega_0 \pm \omega_m$, which are located on either side of the center frequency ω_0 . The deviations might be caused by spurious signals due to oscillator harmonics or mixer products. These appear as discrete spikes in the spectrum, as seen in figure 2.5(a). When the deviations are due to random changes like device thermal noise, it will appear as a broad continuous distribution localized about the center frequency ω_0 , depicted in figure 2.5(b). A combination of both discrete spikes and broad continuous distributions are shown in (c) [2].

Figures 2.3 and 2.5 look the same. From equations 2.7 and 2.10 it is shown that amplitude noise and phase noise exhibit the same power spectrum, although varying in the spectral amplitudes. This makes it impossible to distinguish whether the modulation sidebands are due to amplitude noise or phase noise by just looking at the power spectrum of the signal. Therefore, in order to distinguish between the phase noise and amplitude noise, special measuring techniques must be employed. These measuring techniques are discussed in chapter 3.

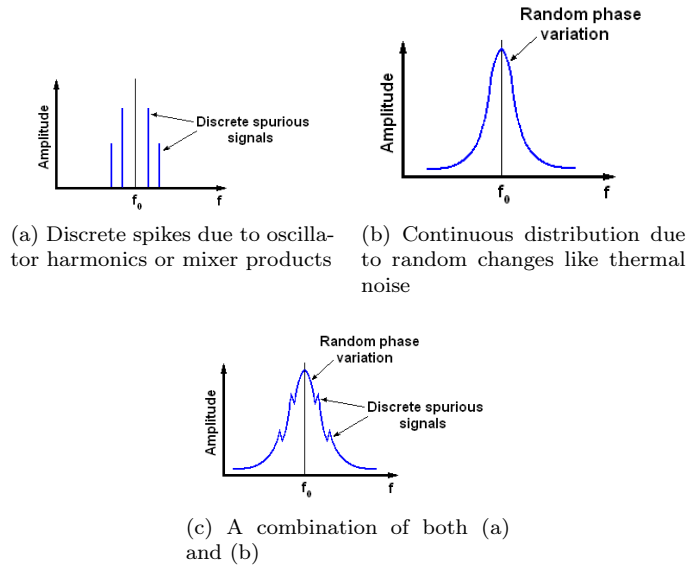


Figure 2.5: Different forms by which phase noise is presented

2.5 Phasor Representation of Amplitude & Phase Noise

Now that phase noise and amplitude noise have been defined mathematically in equations 2.6 and 2.8 in sections 2.3 and 2.4, a phasor can be constructed that shows that contribution of both noise types. Equation 2.1 is presented as a phasor diagram in polar coordinates, as seen in figure 2.6. Amplitude noise gives rise to a random component in the radial direction, while phase noise is responsible for a random component in the polar direction. Note the noise sources illustrated here are sinusoidal, but they can be random in nature. The restricted region where the resulting phasor $v_0(t)$ can be located, remains within the greyed area for any type (random or discrete) of amplitude and phase noise.

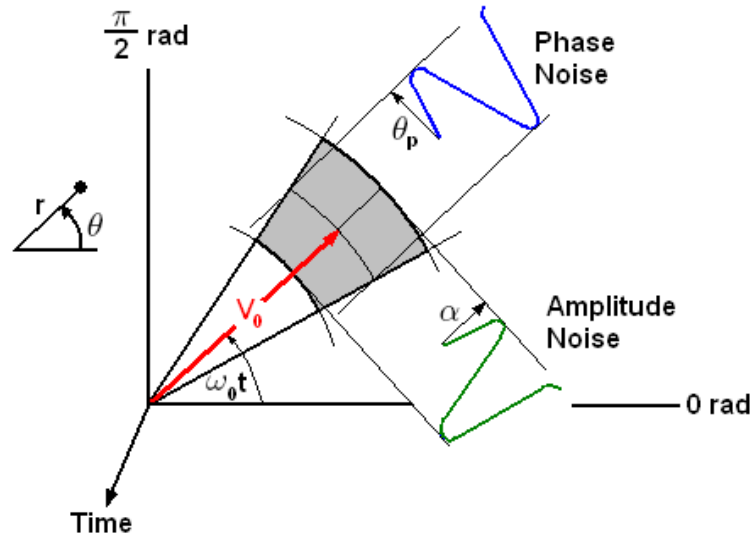


Figure 2.6: Phasor representation of a sinusoid with amplitude- and phase noise

2.6 Characterization of Frequency, Amplitude and Phase Instabilities

Signals can be described in terms of signal power as a function of frequency. This is known as the *power spectrum*, $P(f)$ and is measured in watts $[W]$. Signals are also described in terms of *power spectral density* (PDS), $S(f)$, in dimensions of power per hertz $[W/Hz]$. The spectral density of a signal will, when multiplied by the bandwidth at which the PDS was obtained, give the power per unit frequency contained in the signal. Frequency, amplitude and phase instabilities can be defined or measured by one-sided double-sideband (DSB) spectral densities [4], as have been done in sections 2.6.1, 2.6.2 and 2.6.3.

2.6.1 Amplitude noise

The unit of measure of amplitude noise is the spectral density of normalized amplitude fluctuations, $S_a(f)$, given by [4]

$$S_a(f) = \frac{a_{rms}^2(f)}{BW} \quad [1/Hz] \quad (2.11)$$

where

- $a_{rms}(f)$ - the Fourier transform of the root mean squared $a(t)$ in equation 2.2, measured f hertz away from the carrier
- f - the frequency offset from the carrier
- BW - the bandwidth used to measure $a(t)$ in equation 2.2.

The non-normalized amplitude noise spectral density, $S_A(f)$, is given by

$$S_A(f) = \frac{A_{rms}^2(f)}{BW} \quad [V^2/Hz]$$

where

- $A_{rms}(f)$ - the Fourier transform of the root mean squared $A(t)$ in equation 2.1, measured f hertz away from the carrier
- f - the frequency offset from the carrier
- BW - the bandwidth used to measure $A(t)$ in equation 2.1.

2.6.2 Frequency noise

The unit of measure of frequency noise is the spectral density of normalized frequency fluctuations, $S_y(f)$, given by [4]

$$S_y(f) = \frac{y_{rms}^2(f)}{BW} \quad [1/Hz] \quad (2.12)$$

where

- $y_{rms}(f)$ - the Fourier transform of the root mean squared normalized frequency fluctuations, $y(t)$, in equation 2.3, measured f hertz away from the carrier
- f - the frequency offset from the carrier
- BW - the bandwidth used to measure $y(t)$ in equation 2.3.

The non-normalized frequency noise spectral density, $S_f(f)$, is given by

$$S_f(f) = \frac{\dot{\phi}_{rms}^2(f)}{BW} \quad [Hz^2/Hz]$$

where

- $\dot{\phi}_{rms}(f)$ - the Fourier transform of the of the root mean squared frequency fluctuations, $\dot{\phi}(t)$, in equation 2.1, measured f hertz away from the carrier

- f - the frequency offset from the carrier
 BW - the bandwidth used to measure $\dot{\phi}(t)$ in equation 2.1.

2.6.3 Phase noise

Phase instabilities can be characterized by the spectral density of phase fluctuations, $S_\phi(f)$, given by [4, 5]

$$S_\phi(f) = \frac{\phi_{rms}^2(f)}{BW} \quad [rad^2/Hz] \quad (2.13)$$

where

- $\phi_{rms}(f)$ - the Fourier transform of the root mean squared frequency fluctuations, $\phi(t)$, in equation 2.1, measured f hertz away from the carrier
 f - the frequency offset from the carrier
 BW - the bandwidth used to measure $\phi(t)$ in equation 2.1.

Another useful measure of the phase noise, $\mathcal{L}(f)$, can be defined if the total phase deviations are small ($\phi_{max}(t) \ll 1rad$) and is related to $S_\phi(f)$ by

$$\mathcal{L}(f) = \frac{1}{2} S_\phi(f) \quad (2.14)$$

The NBS (National Bureau of Standards, U.S. Department of commerce) defines $\mathcal{L}(f)$ as the single sideband phase noise relative to the carrier as follows [6]:

$$\mathcal{L}(f) = \frac{P_{SSB}(f)}{P_s} [1/Hz] \quad or \quad \mathcal{L}(f) = 10 \log \left[\frac{P_{SSB}(f)}{P_s} \right] [dBc/Hz] \quad (2.15)$$

where

- $P_{SSB}(f)$ - spectral power density in one phase modulation (PM) sideband, offset f Hz from the carrier
 P_s - total power in noiseless signal
 f - the frequency offset from the carrier
 $[1/Hz]$ - the phase noise has been normalized to power of the carrier, leaving the per Hertz as the parameter specifying the bandwidth in which $P_{SSB}(f)$ was measured
 $[dBc/Hz]$ - decibels relative to carrier per hertz. The ratio of the power in the modulation sideband $P_{SSB}(f)$ to the power in the signal P_s is expressed in a logarithmic scale.

Unlike spectral density phase fluctuations, $S_\phi(f)$, the single sideband phase noise relative to the carrier, $\mathcal{L}(f)$, is a measurement of power [5].

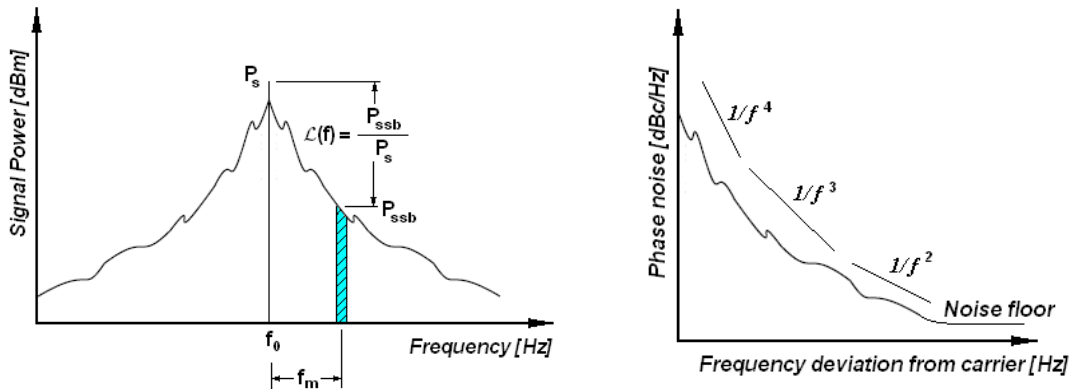
The spectral density phase fluctuations, $S_\phi(f)$, are related to the spectral density frequency fluctuations, $S_f(f)$, in the frequency domain in the following equation [5]:

$$S_\phi(f) = f^2 S_f(f) \tag{2.16}$$

Equation 2.16 is a result of the relation of the phase fluctuations to the frequency fluctuations in the time domain:

$$f(t) = \frac{1}{2\pi} \frac{d}{dt} [\phi(t)] \tag{2.17}$$

Figure 2.7(a) shows how the single sideband phase noise, $\mathcal{L}(f)$, is derived from the double sideband power spectrum $P_s(f)$, relative to the carrier at f_0 . $\mathcal{L}(f)$ is plotted in (b) as the one-sided, single sideband phase noise. The vertical axis is taken at a reference to the carrier amplitude and is expressed in dBc/Hz. The horizontal axis is the deviation from the carrier, in Hertz. Different phase noise sources are approximated by straight lines for parts of the phase noise, $\mathcal{L}(f)$, in (b) with $1/f^n, n \in \mathbb{N}$ [5].



(a) One-sided, double sideband power spectrum, $P_s(f)$. (b) One-sided, single sideband phase noise, $\mathcal{L}(f)$.

Figure 2.7: Frequency domain representations of phase noise.

2.7 Conclusion

In this chapter and introduction to amplitude, phase and frequency instabilities are given.

Section 2.2 briefly introduces the concepts of frequency, phase and amplitude instabilities in the time domain, which are all treated as noise sources. The instabilities are normalized to gain a measure of size of the instabilities.

Sections 2.3 and section 2.4 give mathematical models and a visual representations of amplitude noise and phase noise. It is shown in these two sections that phase noise and frequency noise both lead to sidebands in the frequency domain. The sidebands caused by amplitude noise are indistinguishable from the sidebands caused by phase noise and therefor need to be reduced or eliminated. When designing a phase noise measuring system this problem can be eliminated by removing the amplitude noise within the measuring technique. These techniques are discussed in chapter 3.

Section 2.5 shows how the contribution of both amplitude noise and phase noise can be represented by a rotating phasor.

Finally in section 2.6 the phase, frequency and amplitude instabilities are defined in terms of spectral densities.

Chapter 3

Phase Noise Measurement Methods

3.1 Introduction

A number of different phase noise measuring techniques are discussed in this Chapter. The methods are compared and their feasibility for this project is evaluated. A method is then chosen based on the following goals:

- Large dynamic range.
- Cost effectiveness.
- Equipment availability.
- An equal measuring capability in both close-in and far-out phase noise.
- Ability to measure spurious phase noise as well as continuous distributions of phase noise.

3.2 Normalized Frequency Difference

Phase noise was described in terms of the one-sided, single sideband phase noise, $\mathcal{L}(f)$, in section 2.6.3. This is the representation for phase noise which will be used throughout the rest of the thesis.

Ideally the amplitude noise, $A(t)$, in equation 2.1 is zero for phase noise measurements. There is however always some level of amplitude noise in the oscillator outputs. Generally the amplitude noise can be ignored if it is known to be 10 *dB* less than the phase noise that will be measured [3].

At least two oscillators are generally involved in frequency measurements (except in the frequency demodulation method, section 3.3.5, where only the measured device under test (DUT)

is used). Since frequency measurements are mostly dual (two oscillators involved) it is useful to define the normalized frequency difference as :

$$f_{nor}(t) = \frac{f_{DUT}(t) - f_{LO}(t)}{f_{LO}(t)} \quad (3.1)$$

where

- f_{DUT} - instantaneous frequency of the DUT at time t
- f_{LO} - instantaneous frequency of the LO at time t .

The normalized frequency difference $f_{nor}(t)$ is a dimensionless quantity that shows an oscillators frequency stability performance.

3.3 Phase Noise Measuring Techniques

3.3.1 Spectrum analyzer measurement

The first technique simply measures the output of an oscillator signal (figure 3.1). Both the amplitude noise $S_A(f)$ and the phase noise $S_\phi(f)$ of the oscillator contribute to the sidebands located about the center frequency of the DUT, as discussed at the end of section 2.4. Since this method does not differentiate between phase noise and amplitude noise, it is never used in highly accurate measurements of phase noise.

Feasibility:

- Very easy setup since no design or construction is required.
- Spectrum analyzer available.

Infeasibility:

- This technique is severely limited by phase noise and amplitude noise of the local oscillator (LO) in the spectrum analyzer, which acts as the RO in this measurement setup.
- Close-in phase noise immeasurable.
- High Cost.
- Amplitude noise indistinguishable from phase noise.

Conclusion:

This method can be used to obtain a preliminary view of what the phase noise might look like. Since it does not differentiate between phase noise and amplitude noise, it is not chosen as the measuring method for this project.

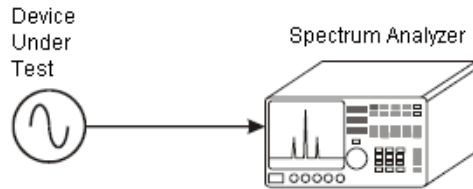


Figure 3.1: Spectrum analyzer phase noise measurement setup

3.3.2 Heterodyne (beat frequency) method

Figure 3.2 shows the heterodyne measurement method. A balanced mixer is used to mix the DUT (f_1), with the RO (f_0). The resulting intermediate frequency (IF) is then passed through a low pass filter (LPF), suppressing the sum frequency, which leaves only the difference frequency, $f_{IF} = |f_1 - f_0|$. The difference frequency, in this case, is known as the beat frequency. After being amplified by a low noise amplifier (LNA), the beat frequency is then measured at a constant rate by a period counter or a frequency counter, as seen in figure 3.2. The normalized frequency difference is then obtained from the beat frequency by use of equation 3.1 as follows:

$$f_{nor}(t_i) = \frac{f_{IF}(t_{i+1}) - f_{IF}(t_i)}{f_1}.$$

From this the one-side single sideband phase noise, $\mathcal{L}(f)$, can be calculated by using a computer.

Feasibility:

- Very good close-in phase noise measurements for the phase noise approximation $1/f^\alpha$ with $\alpha \geq 3$.
- The phase noise of the reference oscillator (RO) can be much better (more than 10dB) than the DUT, in which case the measured phase noise is considered to be only that of the DUT.
- The RO phase noise can also be equal to that of the DUT (for identical oscillators in the DUT and RO). In this case the phase noise measured is equal to the sum of the RO and DUT phase noise, or equivalently twice that of the DUT phase noise.

- Inexpensive components.
- Period and frequency counter available.

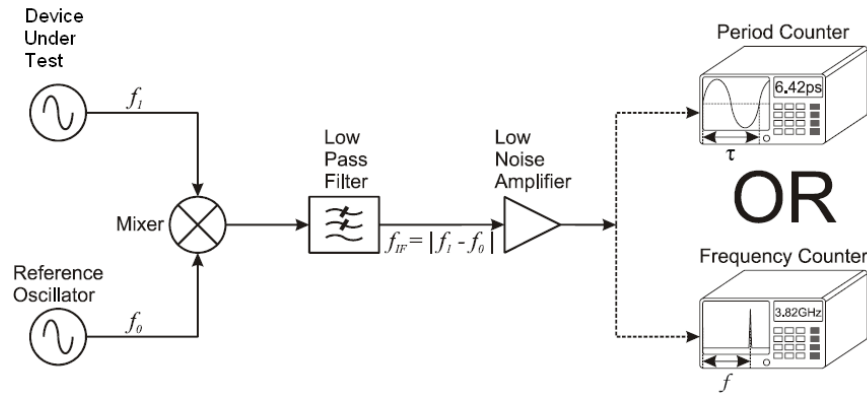


Figure 3.2: Heterodyne (beat frequency) measurement setup

Infeasibility:

- This method is insensitive to spurious phase noise.
- Not suitable for measuring phase noise further away from the carrier, approximated by $1/f^\alpha$ with $\alpha \leq 2$.
- The LO in the period or frequency counter limits the lowest phase noise measurable by the system.

Conclusion:

Even though the heterodyne method can measure essentially all state-of-the-art oscillators, it still performs weakly further away from the carrier. It can also not be used to measure spurious phase noise.

3.3.3 Time difference method

A typical setup for the time difference method is shown in figure 3.3. A time interval counter (equipment that measures the time between positive zero crossings of two signals) is used to measure the time difference between the DUT and the RO. Identical frequency dividers lower the frequency of both the DUT and the RO, thereby increasing the resolution with which the time interval counter can measure the time difference. The time difference (which is the combined

phase noise of the DUT and the RO) between the two beat frequencies is used to calculate one-side single sideband phase noise, $\mathcal{L}(f)$, of the DUT.

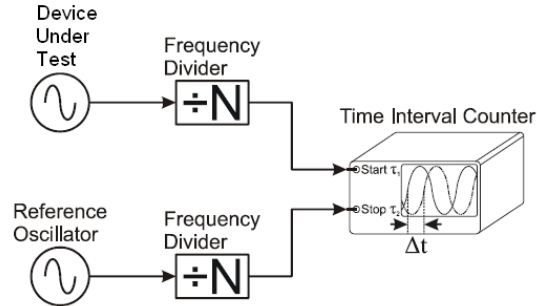


Figure 3.3: Time difference method

Feasibility:

- Simple setup (not a great amount of hardware design required).
- Inexpensive

Infeasibility:

- Great care must be taken regarding cable lengths and impedance matching.
- Since wide bandwidth is needed to measure fast rise-time pulses, this method is limited in bandwidth.
- The LO in the time interval counter limits the lowest phase noise measurable by the system.

Conclusion:

This method lacks the necessary dynamic range to measure very low phase noise. The dual mixer time difference (DMTD) method discussed in the next section improves greatly on accuracy, which makes the DMTD preferable to this one.

3.3.4 Duel mixer time difference system

The DMTD method is a mixture between the heterodyne and the time difference method. Two beat frequencies are formed as $|f_1 - f_0|$ and $|f_2 - f_0|$ by mixing both the DUT and RO with the LO, shown in figure 3.4. The DUT and RO must be the same exact frequency. Usually

atomic standard resonators i.e. cesium, rubidium and hydrogen frequency standards are used. An adjustable phase shifter cancels the starting phase difference between the DUT and the RO. The remaining time difference (which is the combined phase noise of the DUT and the RO) between the two beat frequencies is used to calculate one-side single sideband phase noise, $\mathcal{L}(f)$, of the DUT.

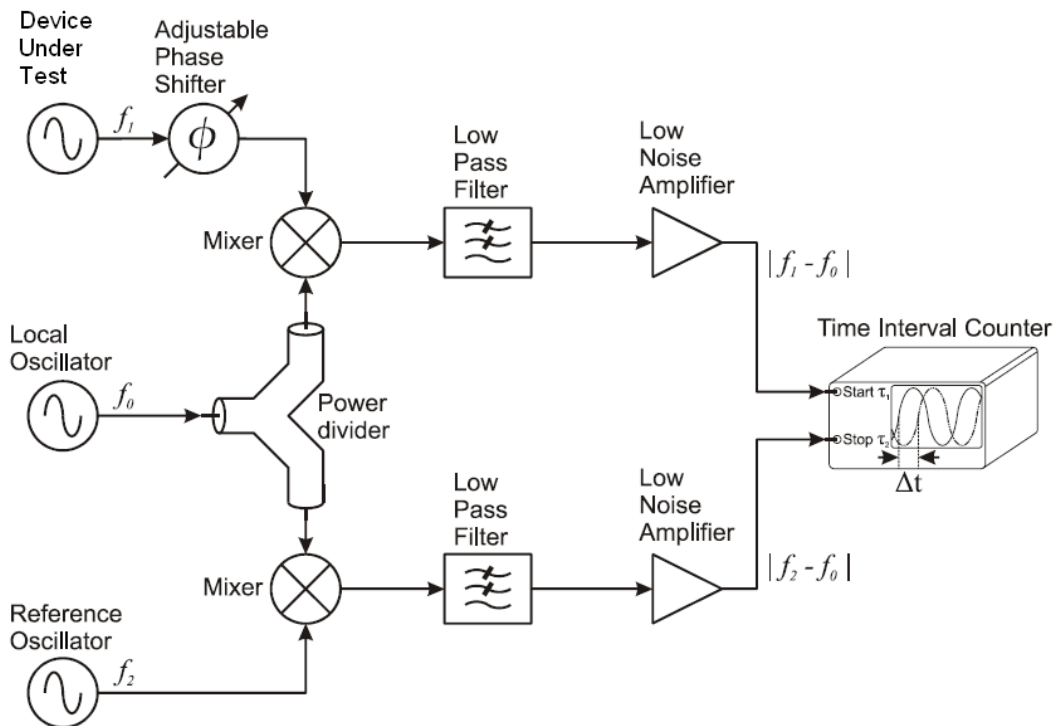


Figure 3.4: Duel mixer time difference method

Feasibility:

- High resolution time domain measurement.
- Inexpensive.

Infeasibility:

- Only atomic standard resonators i.e. cesium, rubidium and hydrogen frequency standards are used.

- The LO in the time interval counter limits the lowest phase noise measurable by the system.

Conclusion:

Since only atomic standard resonator are used, this method is not suited for this project.

3.3.5 Frequency demodulation

A frequency demodulator is shown in figure 3.5. The frequency discriminator strips the DUT signal of the carrier and translates the carrier sidebands (phase noise) to base band. The frequency discriminator used in figure 3.5 is a delay line. Cavity and bridge types are other frequency discriminators that can be used. A low pass filter strips the IF of the frequency sum components. The remaining base band signal is amplified with a LNA and a computer is used to calculate the one-side single sideband phase noise $\mathcal{L}(f)$.

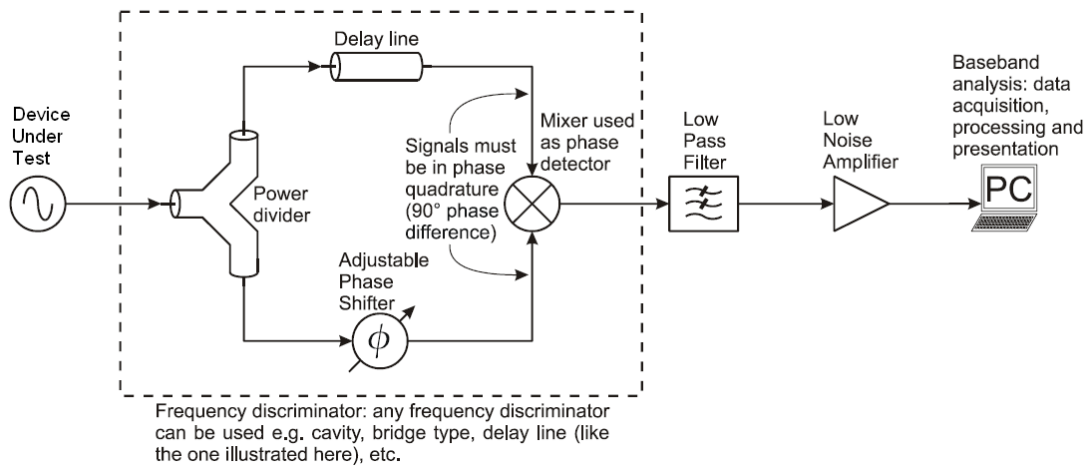


Figure 3.5: Frequency demodulation phase noise measurement method

Feasibility:

- The only method that requires no RO.
- Very good for measuring large phase deviations at slow rates, e.g. free running VCO.
- Inexpensive.

Infeasibility:

- The frequency discriminator is specifically designed for the frequency of the DUT, which means that only a small bandwidth of DUTs can be measured.
- Calibration of the frequency discriminator requires a significant frequency shift in the DUT.
- The system sensitivity degrades as the phase noise is evaluated closer to the carrier.

Conclusion:

Many phase noise measuring methods employ a PLL with a very narrow bandwidth. It can happen that the PLL fails to lock on a free running VCO, due to the narrow bandwidth of the PLL. This method is useful to measure the phase noise of free running VCO's, since no PLL is required. The narrow bandwidth of the frequency discriminator limits the DUT frequencies measurable too much to be considered as the best measuring method for this project. This method is the secondary measuring method of choice.

3.3.6 Phase demodulation

When two signals, which are in phase quadrature, are mixed the resulting IF is the phase difference between the two signals (figure 3.6). This concept is explained mathematically as follow:

$$\begin{aligned}
 e_0(t) &= \cos(\omega_1 t + \phi_1) \times \cos(\omega_2 t + \phi_2 + \frac{\pi}{2}) \\
 &= \cos((\omega_1 - \omega_2)t + \phi_1 - \phi_2 - \frac{\pi}{2}) + \cos((\omega_1 + \omega_2)t + \phi_1 + \phi_2 + \frac{\pi}{2}) \quad (3.2)
 \end{aligned}$$

where

- ω_1, ω_2 - The frequencies of the DUT and RO
- ϕ_1, ϕ_2 - The phase noise of the DUT and RO.

Putting the IF, $e_0(t)$, through a low pass filter removes the sum frequency components:

$$[e_0(t)]_{LPF} = \cos((\omega_1 - \omega_2)t + \phi_1 - \phi_2 - \frac{\pi}{2}) \quad (3.3)$$

With the RO and DUT at the same frequency, $\omega_1 = \omega_2$, $[e_0(t)]_{LPF}$ becomes:

$$[e_0(t)]_{LPF} = \sin(\phi_1 - \phi_2) \quad (3.4)$$

The small angle approximation for a sinusoid, where $\phi_1 - \phi_2 \ll 1rad$, is applied for small phase differences:

$$[e_0(t)]_{LPF} = \phi_1 - \phi_2 \quad (3.5)$$

The resulting phase difference in equation 3.5 is the phase noise contribution of both the DUT and the RO.

In figure 3.6 a mixer is used as a phase detector by ensuring that the input signals, the DUT and the RO, are in exact phase quadrature (90° phase difference). A PLL with a narrow bandwidth keeps the DUT and RO (in this case a VCO) in phase quadrature. The one-side single sideband phase noise, $\mathcal{L}(f)$, is calculated by a computer from the amplified phase difference in equation 3.5.

Feasibility:

- Close-in as well as far-out phase noise measurements can be performed.
- Spurious phase noise can be measured.
- Since the carrier is suppressed a large dynamic range (typically -170 dBc/Hz) is achieved.
- The PLL ensures long term frequency drift between the RO and DUT does not affect the measurement.
- This measurement is inexpensive.

Infeasibility:

- A RO with significantly less phase noise (more than 10 dB) than the DUT is required.
- Identical oscillators are required for the DUT and RO in the case where the phase noise of the DUT is unknown.
- Phase noise measurements at a lower frequency than the loop bandwidth of the PLL need to be compensated for mathematically. These measurements are treated as frequency demodulation.

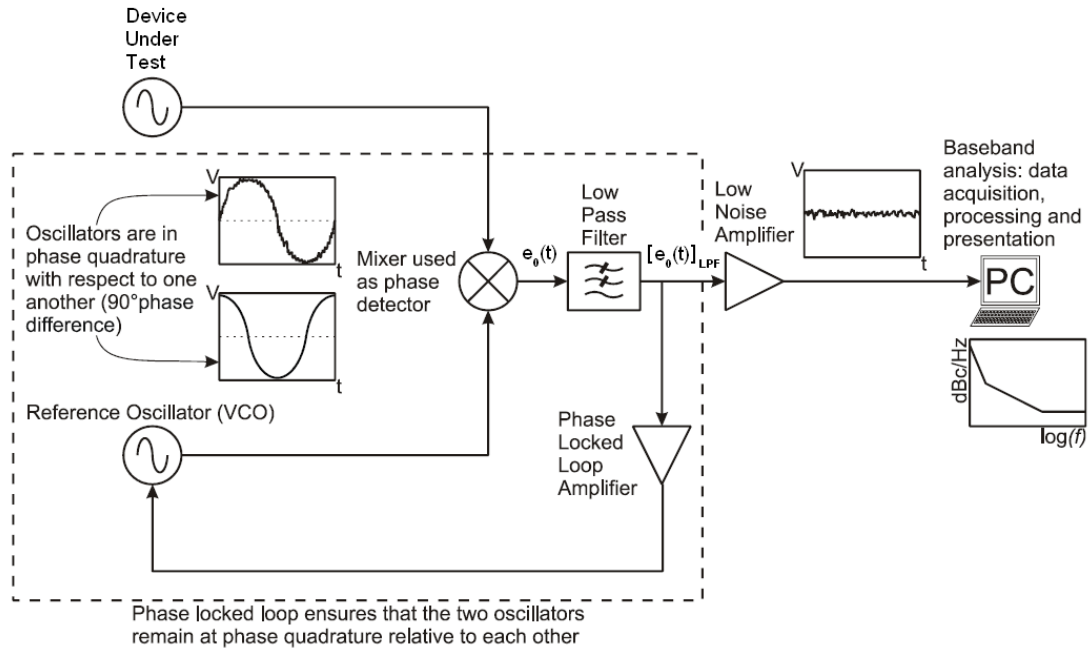


Figure 3.6: Phase demodulation phase noise measurement method

Conclusion:

This is the measurement method chosen for this project. It is an inexpensive and highly accurate measurement technique which is relatively simple to implement. The only additional equipment required is a personal computer and some form of analog to digital conversion.

3.4 Conclusion

In this chapter measuring methods were discussed as to their viability for implementation in this project. The qualities of the phase demodulation measuring technique from section 3.3.6 neatly coincides with the requirements of this project. Therefore, the phase demodulation method is the method of choice.

Chapter 4

Hardware

4.1 Introduction

The phase demodulation method is chosen for this project. This chapter discusses all the hardware design specifications needed to implement the phase demodulation method. A modular approach is taken in designing the phase noise measuring system by dividing the design into the following separate hardware components:

- PLL
- LNA Prefilter
- LNA
- LNA Output LPF
- Analog to digital converter (ADC) Prefilters

Each of the hardware components are designed, simulated and measured separately (without being connected to the rest of the measuring system). The effects of connecting all the hardware components to form the complete measuring system is discussed in Chapter 6. By using a modular approach the hardware components become interchangeable. Measuring the phase noise of oscillators that fall outside the limits of the measuring system developed in this thesis does not require a whole system redesign. Only certain hardware components need to be redesigned.

4.2 Hardware Design Specifications

The following section discuss how the phase demodulation method is applied. The design specifications are also discussed.

The phase noise bandwidth of interest ranges from 10 Hz to 10 MHz away from the carrier signal. The DUT which phase noise is being measured has a frequency of 10 MHz . The VCO must accordingly also have a frequency of 10 MHz so that the mixer will mix the measured phase noise down to base band.

The PLL imposes the lower frequency limit by having a bandwidth of 10 Hz . To ensure a zero steady state tracking error of the PLL an integrator is needed in the PLL filter. Section 4.3.2 explains why this is important.

Before the phase error (measured phase noise) $e_0(t)$ can be amplified by the LNA, the sum frequency component must be removed (equation 3.3). This is accomplished with the LNA Prefilter, which has a -3 dB low pass frequency of 10 MHz . The LNA Prefilter also suppresses the 10 MHz carrier signals from the VCO or DUT that might leak through the mixer.

The LNA amplifies the measured phase noise by a variable gain of 26 dB , 52 dB or 78 dB .

A LNA output filter limits the noise generated by the LNA to 10 MHz .

After amplification and filtering, the phase noise is ready to be processed for sampling. The phase noise bandwidth 10 Hz to 10 MHz is split into three bands before sampling. Doing so results in more resolution at lower frequencies, as explained in section 4.7. The three bands are listed in table 4.4. Figure 4.1 is an overview of the design specifications.

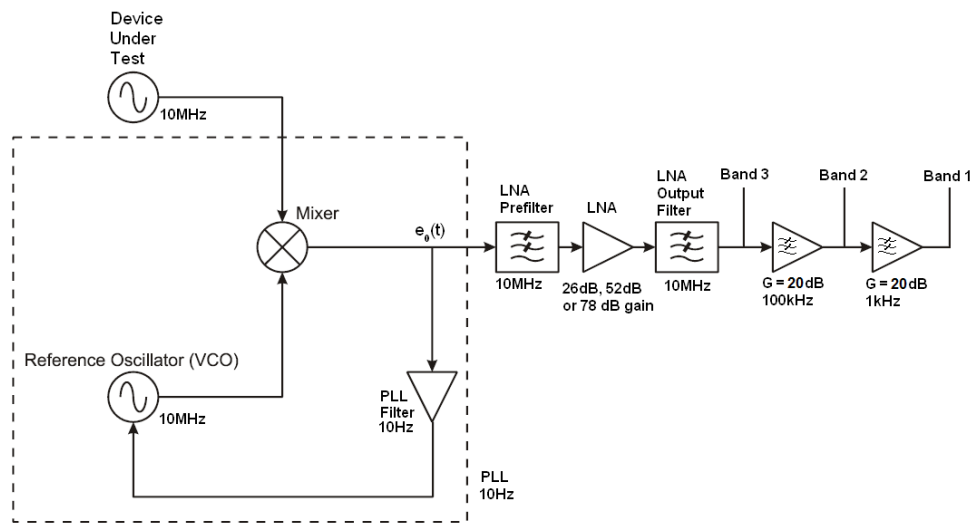


Figure 4.1: Adapted phase demodulation method with hardware design specifications.

4.3 PLL

4.3.1 Introduction

The phase demodulation measurement method from section 3.3.6 starts with a phase locked loop (PLL). The phase locked loop is responsible for creating the voltage phase error $e_0(t)$, which is the combined phase noise of the DUT and the VCO. Figure 4.2 shows the typical feedback system of a PLL [7].

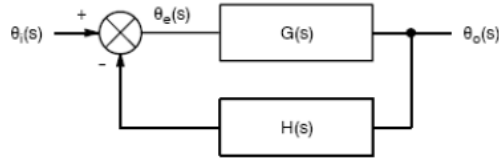


Figure 4.2: Phase Locked Loop feedback system

The parameters of figure 4.2 are defined as follow:

- $\theta_i(s)$ - phase input in degrees
- $\theta_e(s)$ - phase error in degrees
- $\theta_o(s)$ - output phase in degrees
- $G(s)$ - product of the feed forward transfer functions
- $H(s)$ - product of the feedback transfer functions.

The following relationships are obtained from servo theory [7]:

$$\theta_e(s) = \frac{1}{1 + H(s)G(s)} \theta_i(s) \quad (4.1)$$

$$\theta_o(s) = \frac{G(s)}{1 + H(s)G(s)} \theta_i(s) \quad (4.2)$$

The transfer functions of a PLL can be substituted for the parameters $H(s)$ and $G(s)$ as shown in figure 4.3.

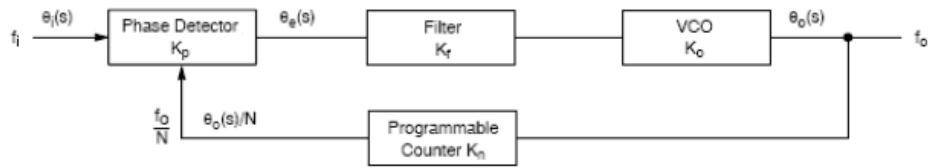


Figure 4.3: PLL with substituted parameters.

The phase detector generates a voltage at its output $\theta_e(s)$, which is proportional to the phase difference between its inputs $\theta_i(s)$ and $\theta_o(s)/N$. This voltage signal, after filtering, is then used as a control signal for the VCO. The phase detector, filter and the VCO comprise the feed forward transfer function $G(s)$. The feedback path $H(s)$ contains a programmable counter. In this thesis the programmable counter is omitted and unity gain is substituted instead ($N = 1$). The feed forward and feedback transfer functions are given by:

$$G(s) = K_p \cdot K_f \cdot K_o \quad H(s) = K_n \quad (4.3)$$

where

$$K_n = \frac{1}{N} = 1 \quad (4.4)$$

4.3.2 Components

DUT

The DUT generates $\phi_i(s)$ in figure 4.3, which contains the phase noise that is measured. Two sources are measured in this project: the Marconi Instruments 2019A 80 kHz - 1040 MHz signal generator and a leaded 10 MHz voltage controlled crystal oscillator (VCXO) from IQD Frequency Products. Using the VCXO as a DUT requires that the voltage reference be biased in the middle of VCXO operating curve (figure 4.7) by use of a resistive voltage divider circuit.

Phase Detector

A double balanced mixer with no charge pump, the ADE-2 is used as a phase detector. Double balanced refers to the high isolation between both mixer inputs to the mixer output. Therefore choosing a double balance mixer ensures good isolation between the mixer inputs and mixer output. Isolation is ≥ 55 dB for the ADE-2 when both the LO and RF are at 10 MHz. A mixer can be modeled by figure 4.4:

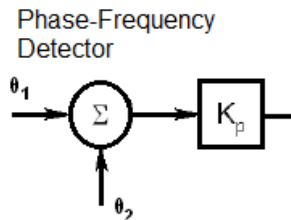


Figure 4.4: Typical model of a mixer

This can also be represented by the following equation:

$$K_p[\cos(\phi_1) \times \cos(\phi_2)] = K_p \cos(\phi_1 + \phi_2) + K_p \cos(\phi_1 - \phi_2) \quad (4.5)$$

where

- K_p - mixer gain in Volt/radians
- θ_1, θ_2 - the respective phase of each input signal, in degrees.

The mixer gain K_p is not specified in the data sheet for the ADE-2 [8]. In order to acquire a value for K_p two VCXOs are mixed. Both VCXOs have a power output of 10 dBm and they are both set up to produce constant, but slightly different frequencies. The output signal of the mixer is then driven through a low pass filter that has a parallel capacitive element first. The next paragraph explains why a parallel capacitive element first is important at the output of the mixer. The low pass filter strips the mixer output of the sum frequencies $K_p \cos(\phi_1 + \phi_2)$, leaving only the difference frequencies $K_p \cos(\phi_1 - \phi_2)$. This is expressed in equation 4.6. An example where K_p is measured for the ADE-2 is shown in figure 4.5.

$$\{K_p[\cos(\phi_1) \times \cos(\phi_2)]\}_{LPF} = K_p \cos(\phi_1 - \phi_2) \quad (4.6)$$

The mixer gain K_p is determined by using the gradient through the zero crossing (between the vertical markers) on the positive slope of the difference frequencies in figure 4.5. The gradient is calculated as follow:

$$\begin{aligned} K_p &= \frac{dV}{d\phi} \\ &= \frac{600 \text{ mV}}{(2\pi 3.35 \text{ kHz}) \times 100 \mu\text{s}} \\ &= 285.05 \text{ mV/rad} \end{aligned} \quad (4.7)$$

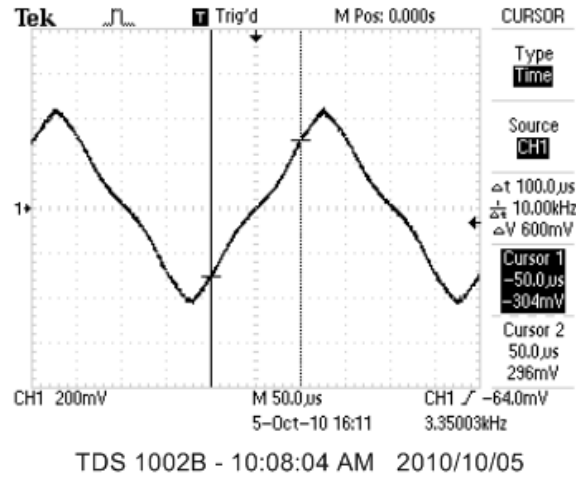


Figure 4.5: Two 10 MHz VCXO signals are mixed and filtered, resulting in the difference frequencies $K_p \cos(\phi_1 - \phi_2)$.

The mixer gain K_p is experimentally found to be independent of the mixed signal's frequencies. However, it is dependent on the power of the input signals (all DUT power levels used in this project are 10 dBm) as well on the load impedance at the output of the mixer. The low pass filter (LNA Prefilter) connected to the mixer output in figure 4.1 can have either an inductive series element first, or a capacitive parallel element first, which affects the input impedance of the filter. By simulating in LT Spice for both the cases it is determined that the mixer responds favorably to the capacitive parallel element first as the gain K_p of the mixer is higher for this case. Higher mixer gain is favorable as it increases signal to noise ratio of the measured phase noise (where phase noise is considered to be the signal in this case). A higher signal to noise ratio means that smaller phase noise will be measurable by the measuring system. Figure 4.6 illustrates these simulations.

The parallel capacitive element first in the figure shows a more non-linear response than the series inductor first, but the in-phase-point (top peak) is higher than that of the series inductive element first. Since the phase noise that will be measured will be small (close to the zero crossings) the linear triangle shape of the inductor load is not needed. Therefore the LNA Prefilter, which is connected to the mixer output, is designed with a capacitive parallel element first in section 4.4.

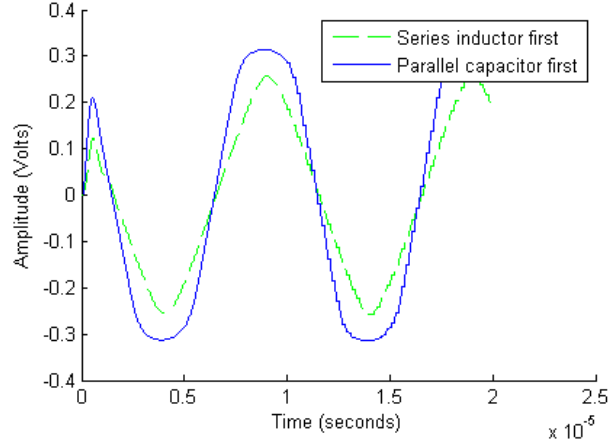


Figure 4.6: LT Spice simulation results illustrating the different mixer gains K_p for the two cases of series inductor first or parallel capacitor first at the output of the mixer.

VCO

In this thesis a leaded 10 MHz VCXO from IQD Frequency Products is implemented as the VCO. The transfer function of a VCO is given by:

$$K_o = \frac{K_{VCO}}{s} \quad (4.8)$$

where K_{VCO} is the sensitivity gain of the VCO in radians per second per volt. The denominator in equation 4.8 acts as an integrator, which converts the frequency characteristics of the VCO into phase. The VCO sensitivity gain is found by using the curve in figure 4.7 [9] in conjunction with the following equations:

$$\begin{aligned} K_{VCO} &= \frac{1kHz - (-1kHz)}{3.8V - 0.9V} \cdot 2\pi \text{ rad/s/V} \\ &= 4.333 \times 10^3 \text{ rad/s/V} \end{aligned} \quad (4.9)$$

Thus

$$K_o = \frac{4.333 \times 10^3}{s} \text{ rad/s/V} \quad (4.10)$$

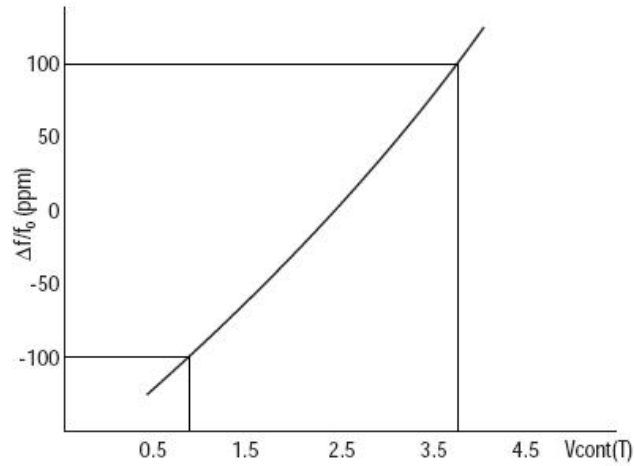


Figure 4.7: VCO sensitivity curve for the leaded 10 MHz VCXO from IQD Frequency Products

PLL Filter

There are various types and orders of PLLs. The *type* refers to the number of poles of the loop transfer function $H(s)G(s)$ in equation 4.1 which are located at the origin. The following is an example of a *type one* system since there is only one pole located at the origin [7]:

$$G(s)H(s) = \frac{10}{s(s+10)} \quad (4.11)$$

The *order* of the system refers to the highest degree of the characteristic equation (C.E.). The C.E. of equation 4.11 is determined as follow:

$$1 + G(s)H(s) = 1 + \frac{10}{s(s+10)} = 0 \quad (4.12)$$

Therefore

$$C.E. = s^2 + 10s + 10 \quad (4.13)$$

which is a *second order* polynomial. To summarize, the transfer function $H(s)G(s)$ in equation 4.11 is an example of a *type 1 second order* system.

The resulting steady state phase error θ_e in figure 4.3 depends on the *type* of the PLL transfer function $H(s)G(s)$.

By using table 4.1 [7], it is determined that the minimum system type needed for a PLL to track a reference frequency (step velocity) with zero phase error, is of type 2. A zero steady

state error is required so as not to saturate the LNA in figure 4.1 with a direct current (DC) voltage. A constant steady state error presents itself as a DC voltage at the output of the phase detector.

Table 4.1: Steady state phase errors θ_e for various system types

	Type 1	Type 2	Type 3
Step Position	Zero	Zero	Zero
Step Velocity	Constant	Zero	Zero
Step Acceleration	Continually increasing	Constant	Zero

A common PLL transfer function of *type 2* is given by [7]:

$$G(s)H(s) = \frac{(s+a)K}{s^2} \quad (4.14)$$

This transfer function is of second order and is the transfer function used to design the PLL in this thesis. A zero is added at $s = -a$ in order to provide the loop with stability. Without the zero the root locus poles would move along the $j\omega$ axis as a function of gain and always be in an oscillatory state. The root locus of equation 4.14 is shown in figure 4.8. As seen from the root locus the added zero provides stability.

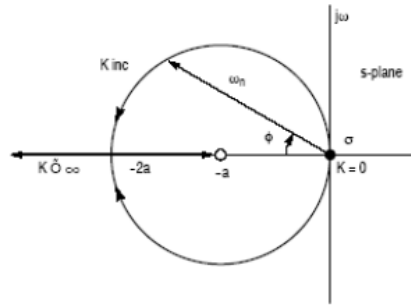


Figure 4.8: Type 2 second order root locus of $G(s)H(s) = \frac{(s+a)K}{s^2}$.

Equation 4.14 is related to equation 4.3 in the following manner:

$$G(s)H(s) = \frac{(s+a)K}{s^2} = K_p \cdot K_f \cdot K_o \cdot K_n \quad (4.15)$$

With K_p , K_o and K_n already defined, the PLL filter K_f must take the form

$$K_f = \frac{s + a}{s} \quad (4.16)$$

to provide the zero and pole required to satisfy equation 4.15. The non-inverting operational amplifier configuration shown in figure 4.9 represents the PLL filter in equation 4.16.

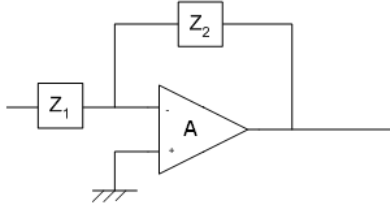


Figure 4.9: Active PLL filter design

The PLL filter becomes

$$K_f = \frac{Z_2}{Z_1} = \frac{R_2Cs + 1}{R_1Cs} \quad \text{for large } A \quad (4.17)$$

where

- A - open loop voltage gain of the operational amplifier
- R_1, R_2 - resistors
- C - a capacitor.

4.3.3 PLL Bandwidth

The bandwidth of the PLL transfer function in equation 4.14 is calculated as follow [7]:

$$\omega_{-3dB} = \omega_n(1 + 2\delta^2 + \sqrt{2 + 4\delta^2 + 4\delta^4})^{1/2} \quad (4.18)$$

Where

- δ - damping ratio
- ω_n - natural frequency in rad/s

Designing for a PLL bandwidth of 10 Hz ($\omega_{-3dB} = 2\pi \cdot 10$) that is critically damped ($\delta = 1/\sqrt{2}$) gives

$$\omega_n = \frac{\omega_{-3dB}}{(1 + 2\delta^2 + \sqrt{2 + 4\delta^2 + 4\delta^4})^{1/2}} = 30.528 \text{ rad/s} \quad (4.19)$$

4.3.4 Complete circuit model

The values for K_p , K_f , K_o and K_n from equations 4.7, 4.17, 4.10 and 4.4 can now finally be substituted into figure 4.3 and is displayed in figure 4.10.

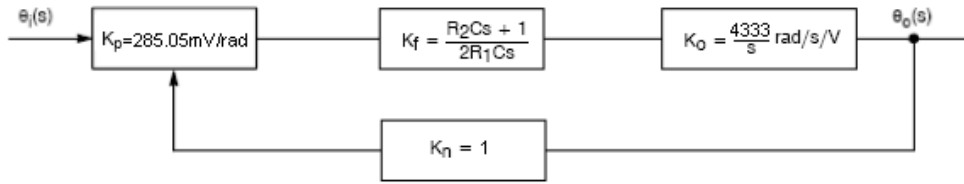


Figure 4.10: Laplace representation of PLL with substituted values for figure 4.3.

The PLL transfer function becomes

$$G(S)H(s) = K_p \left(\frac{R_2 C s + 1}{R_1 C s} \right) \left(\frac{K_{VCO}}{s} \right) K_n \quad (4.20)$$

The C.E. takes the form

$$\begin{aligned} C.E. &= 1 + H(s)G(s) = 0 \\ &= s^2 + \frac{K_p \cdot K_o \cdot K_n R_2}{R_1} \cdot s + \frac{K_p \cdot K_o \cdot K_n}{R_1 C} \end{aligned} \quad (4.21)$$

Relating the C.E. to the standard form

$$s^2 + \frac{K_p \cdot K_o \cdot K_n R_2}{R_1} \cdot s + \frac{K_p \cdot K_o \cdot K_n}{R_1 C} = s^2 + 2\delta\omega_n s + \omega_n^2 \quad (4.22)$$

Equating the coefficients and solving for R_1 and R_2 respectively gives

$$R_1 = \frac{K_p \cdot K_o \cdot K_n}{C\omega_n^2} \quad (4.23)$$

and

$$R_2 = \frac{2\delta\omega_n R_1}{K_p \cdot K_o \cdot K_n} = \frac{2\delta}{C\omega_n} \quad (4.24)$$

The values for ω_n and δ are determined in section 4.3.3. By choosing a value for the capacitor $C = 10 \mu F$, resistors R_1 and R_2 are calculated to be $132.53 k\Omega$ and $4.63 k\Omega$. If C is chosen too large or too small, R_1 and R_2 would become impractical values. Rounding these values to the nearest implementable values gives $R_1 = 130 k\Omega$ and $R_2 = 4.7 k\Omega$.

4.3.5 Simulation of PLL

The PLL transfer function $H(s)G(s)$ in equation 4.20 is the open loop transfer function of the PLL. The bode plot for the open loop transfer function is simulated in *Matlab R2007a* for the calculated values in section 4.3.4. The resulting open loop bode plot is shown in figure 4.11. The $10.13 Hz$ bandwidth of the open loop transfer function is indicated on the bode plot at $-3.009 dB$ and is acceptable. A 90° phase shift at higher frequencies due to the integration is also noticed from the figure. This indicates that the integrator in $H(s)G(s)$ is functioning correctly.

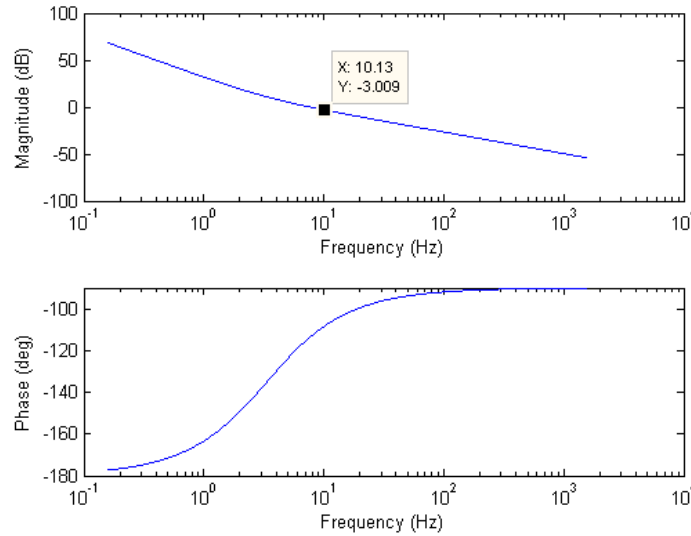


Figure 4.11: PLL open loop simulation bode plot

Figure 4.12 illustrates the PLL closed loop transfer function of equation 4.2. The bode plot for the closed loop transfer function is simulated in *Matlab R2007a* for the values in section

4.3.4. A closed loop bandwidth of 9.74 Hz is read off from the bode plot at -3.01 dB and is acceptable.

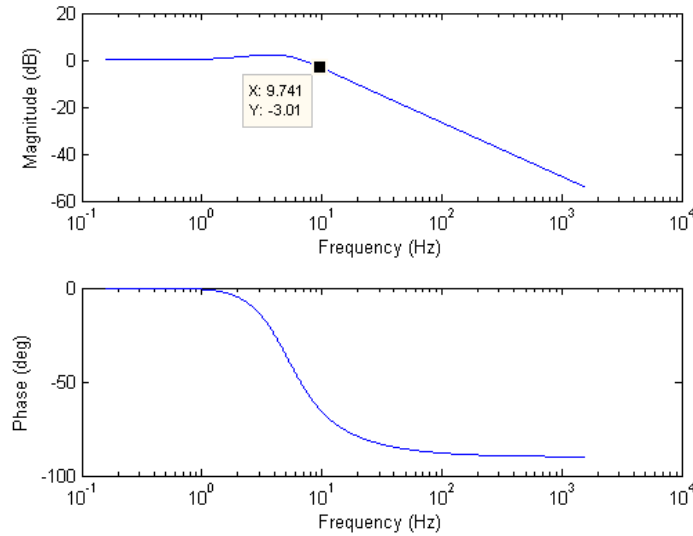


Figure 4.12: Phase locked loop closed loop simulation bode plot

4.3.6 Measurement of PLL bandwidth

In order to measure the bandwidth of the PLL, two 10 MHz VCXOs are used. Measuring of the PLL bandwidth is accomplished by use of a test signal V_x which is applied to the voltage control pin of VCO 1 in figure 4.13. The test signal's amplitude is kept very small for frequencies below 10 Hz (less than $5 mV_{p-p}$). The amplitude must be increased slowly once its frequency is larger than 10 Hz , otherwise the V_y would be too small to measure. VCO 1 frequency modulates the signal V_x , which turns θ_i into a frequency modulated signal. The PLL demodulates θ_i into V_y . The PLL bandwidth is determined by measuring both V_x and V_y while V_x is swept over different frequencies. The closed loop transfer function for the PLL is shown in the following equation:

$$\frac{V_y}{V_x} = \frac{G(s)}{1 + H(s)G(s)}$$

Figure 4.14 shows the measured closed loop amplitude response for the PLL. The closed loop bandwidth is measured as 11 Hz at approximately -3 dB , which is within a satisfactory 10% of the simulated bandwidth in figure 4.12.

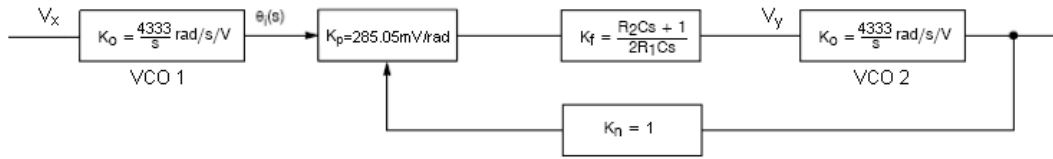


Figure 4.13: Measuring the PLL bandwidth

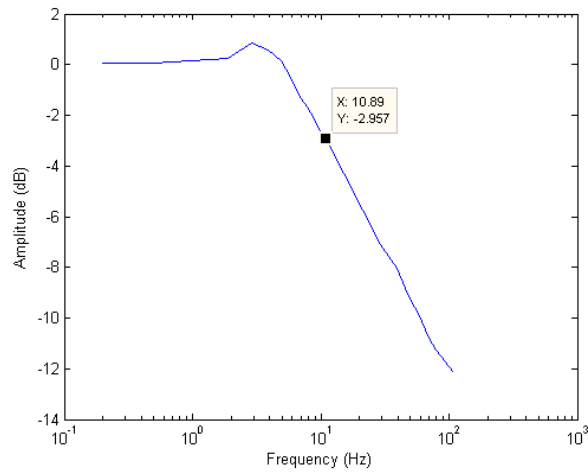


Figure 4.14: PLL closed loop amplitude response

4.3.7 Conclusion

The successful design, simulation and measurement of the constructed PLL is discussed in this section. The close loop bandwidth of the PLL is measured at 11 Hz , which is close enough to the design specification of 10 Hz .

4.4 LNA Prefilter

4.4.1 Introduction

Before the phase error ϕ_e in figure 4.1 can be amplified by the LNA, the sum frequency component must be removed by a LPF, as has been done in equation 4.6. So as not to corrupt ϕ_e with

additional noise, it is driven through a passive LPF to strip it of the sum component. Active filtering would add additional noise to ϕ_e and is therefore avoided.

From section 4.2 the initial design specification of the LNA Prefilter bandwidth is 10 MHz . To minimize the risk of causing the LNA to oscillate, the LNA Prefilter bandwidth is initially limited to 1 MHz . Since the hardware in this project is designed in a modular fashion the 1 MHz LNA Prefilter can be replaced by a 10 MHz LNA Prefilter at a later stage, should it be required to measure phase noise further away from the carrier than 1 MHz .

The output impedance of the mixer is unknown as the mixer contains non-linear components such as diodes. A standard characteristic impedance of $50\ \Omega$ is chosen for the LPF. A Butterworth filter response is chosen for its maximally flat amplitude response.

The LNA that follows the LNA Prefilter is a voltage amplifier circuit. It is therefore of interest for the LNA Prefilter to have maximum voltage transfer between itself and the LNA. To achieve maximum voltage transfer, the filter side facing the LNA is made open-ended (very high characteristic impedance), while the side facing the mixer is $50\ \Omega$ matched. A filter which exhibits such behavior is called a single loaded filter.

4.4.2 LNA Prefilter design & simulation

The standard normalized fifth order Butterworth LPF is read off from the standard tables as:

$$Z_{21}(s) = \frac{K}{s^5 + 3.2361s^4 + 5.2361s^3 + 5.2361s^2 + 3.2361s + 1} \quad (4.25)$$

Applying Cauer 1 five times to equation 4.25 delivers the normalized fifth order single loaded Butterworth LPF in figure 4.15 [10].

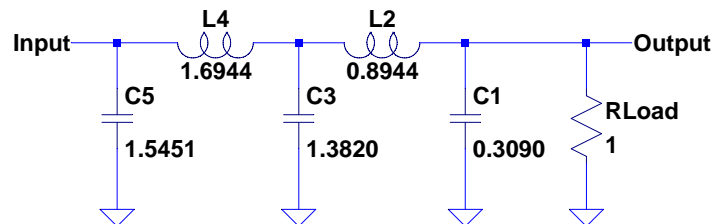


Figure 4.15: Normalized $1\ \Omega$, 1 Hz fifth order single loaded passive Butterworth LPF

For a given load impedance $R_{Load} = 50\ \Omega$, equations 4.26 and 4.27 are used to determine the final filter component values in figure 4.16.

$$C = \frac{C_n}{2\pi f_c R_{Load}} \quad (4.26)$$

$$L = \frac{L_n R_{Load}}{2\pi f_c} \quad (4.27)$$

where

- L_n - is the normalized inductance in H
- C_n - is the normalized capacitance in F
- f_c - is the -3 dB filter cutoff frequency in Hz
- R_{Load} - is the filter characteristic impedance of the loaded sided in Ω .

Designing the filter with a cutoff of 1 MHz gives a simulated (in LT Spice) cutoff frequency of about 900 kHz . To compensate for the lower cutoff frequency, the filter in figure 4.16 is designed with a cutoff frequency of 1.1 MHz . The capacitor values have been rounded to the nearest practical implementable values.

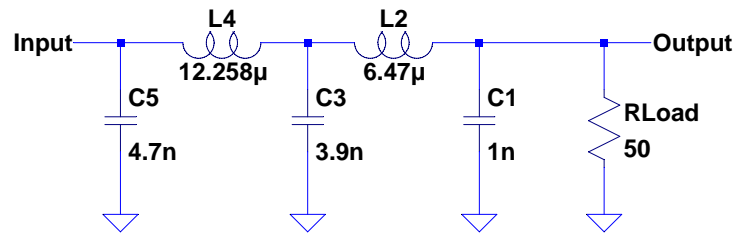


Figure 4.16: 1 MHz , $50\ \Omega$ fifth order single loaded Butter worth passive LPF

The simulated cutoff frequency is read off from simulated amplitude response in figure 4.17.

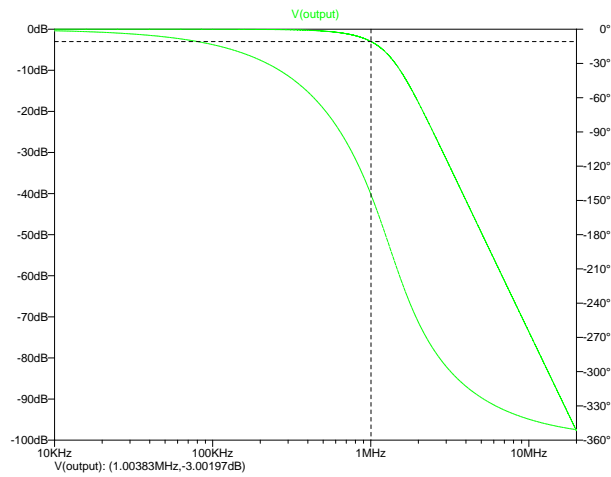


Figure 4.17: Simulated (in LT Spice) amplitude response for a 1MHz , $50\ \Omega$ fifth order single loaded passive Butter worth LPF

4.4.3 Measurement

The filter designed in section 4.4.2 is constructed. The amplitude response is measured by applying a 0 dB frequency sweep signal to the input of the filter in figure 4.16. The output is measured and plotted in figure 4.18. A -3 dB cutoff frequency of 1.02 MHz is determined from the figure which is close to the simulated 1 MHz .

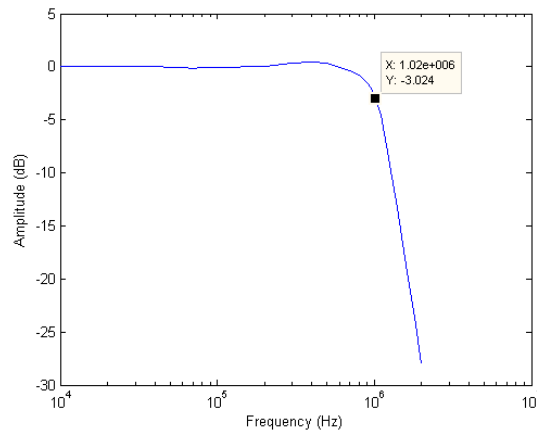


Figure 4.18: Measured amplitude response for the 1 MHz , $50\ \Omega$ fifth order single ended passive Butter worth LPF

4.4.4 Conclusion

The successful design, simulation and construction of the LNA Prefilter is discussed in this section. The LNA Prefilter succeeds in stripping the output of the mixer of the sum frequency component by limiting the LNA input bandwidth to 1 *MHz*.

The filter is connected to the mixer with its loaded side. The open ended side of the filter is connected to the LNA to ensure maximum voltage transfer from the filter to the LNA.

4.5 LNA

4.5.1 Introduction

Once the phase detector in the PLL of section 4.3 has generated the phase error θ_e (figure 4.3), the phase error needs to be amplified so that it is measurable by the ADC. To prevent excess noise from degrading the phase noise measurement, a LNA is needed. Using a LNA results in a larger dynamic range of the measurement system. The LNA is designed for a total gain of 78 *dB*. The gain is achieved through three amplification stages, each of which consists of a non-inverting operational amplifier circuit with a gain of 26 *dB*. The design, simulation and measurement of the LNA is discussed in this section.

4.5.2 LNA Design

The LNA is designed in such a manner as to supply a large gain while trying to minimize its own additive voltage noise. The root mean square (RMS) thermal noise voltage generated by a resistor is given in the following equation [1]:

$$V_n = \sqrt{4kBT R} \quad [V_{rms}] \quad (4.28)$$

where

- k - the Boltzmann's constant in joules per kelvin
- T - the resistor's absolute temperature in kelvin
- R - the resistance in ohm.

From equation 4.28 can be seen that smaller resistance results in smaller thermal noise generated by that resistor. Therefore resistor values are kept as small as possible, especially in the first operational amplifier, to keep their thermal noise contributions small.

Figure 4.19 shows the complete circuit diagram of the LNA. The bandwidth of the PLL is measured at 11 *Hz* in section 4.3.6. This means that only alternating current (AC) signals larger than 11 *Hz* are amplified by the LNA.

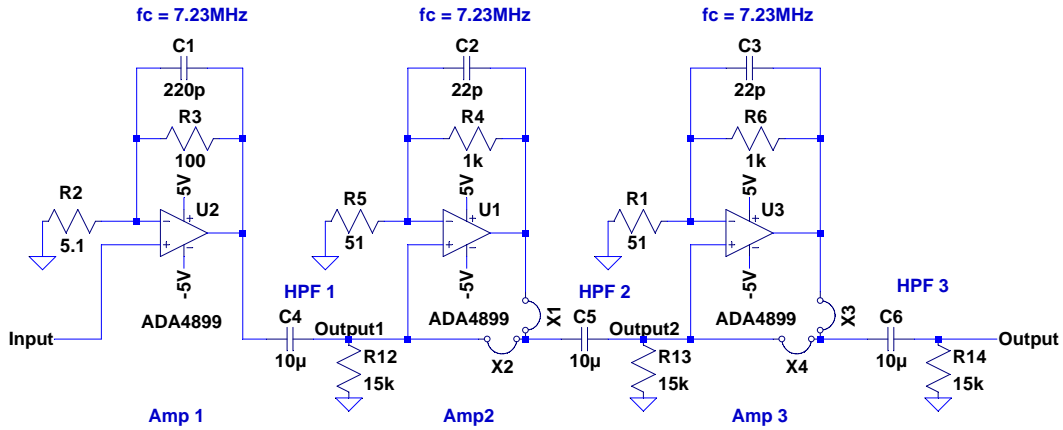


Figure 4.19: LNA circuit diagram

The operational amplifier used in the LNA for each of the amplifiers in figure 4.19 is the ultra low noise ADA4899-1 op-amp from Analog Devices. The ADA4899-1 is chosen for its superior low noise and large bandwidth characteristics. It has a input referred voltage noise of $1\text{ nV}/\sqrt{\text{Hz}}$, a -3 dB unity gain bandwidth of 600 MHz and an input bias current of $1.5\text{ }\mu\text{A}$ (with the condition that the disable pin be connected to $+V_S$).

The internal operational amplifier bandwidth due to the gain of 26 dB can be estimated from the graph in figure 4.20 to be approximately 12 MHz [11].

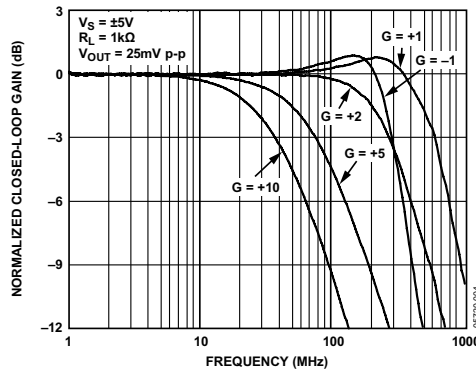


Figure 4.20: ADA4899-1 Small signal frequency response for various gains

The bandwidth of each amplification stage is further limited by the feedback capacitors C_1 , C_2 and C_3 to 7.23MHz (oscillations occurred at 8.2MHz and a 7.23MHz bandwidth prevented that). Limiting the bandwidth minimizes the chances for oscillations to occur in the LNA. This bandwidth can be increased at a later stage, should it be required to measure phase noise further away from the carrier.

Jumper switches are placed at X_1 , X_2 , X_3 and X_4 in figure 4.19 so that the second- and/or the third amplifier can be bypassed, effectively reducing the total LNA gain by 26dB or 52dB as needed.

High pass filters (DC-blocks), each with a -3dB cutoff frequency of 1.06Hz , are introduced after each of the different amplifier stages to stop any DC voltages from saturating the operational amplifiers. C_4 and R_{12} comprises high pass filter (*HPF* 1), C_5 and R_{13} comprises *HPF* 2 and finally C_6 and R_{14} comprises *HPF* 3. The phase error θ_e that is amplified by the LNA does not contain any DC voltage. The DC voltage discussed here originates from the input bias current at *Amp 1* that flows through the LPF before it (see figure 4.1). *HPF 1* strips the *Amp 1* output of DC voltage. Ironically, the input bias current of *Amp 2* flows through R_{12} of *HPF 1* and creates a voltage over it:

$$V_{R_{12}} = 1.5\mu\text{A} \times 15\text{k}\Omega = 22.5\text{mV} \quad (4.29)$$

which is amplified by *Amp 2* to 450mV . Once again the DC voltage is removed from the signal by a HPF, in this case *HPF 2*. The pattern is repeated for the rest of the LNA as seen in figure 4.19.

4.5.3 Simulation

An AC sweep simulation from 100mHz to 100MHz is performed in LT Spice on the LNA circuit in figure 4.19. Figure 4.21 shows the amplitude response at the output of *Amp 1*. The -3dB cutoff frequencies are 1.06Hz for the lower limit (high pass) and 5.21MHz for the upper limit (low pass). These cutoff frequencies are different from the designed values. The reduction in bandwidth happens when the three separately designed filters are put back to back. A gain of 26.26dB for *Amp 1* is read off from figure 4.21.

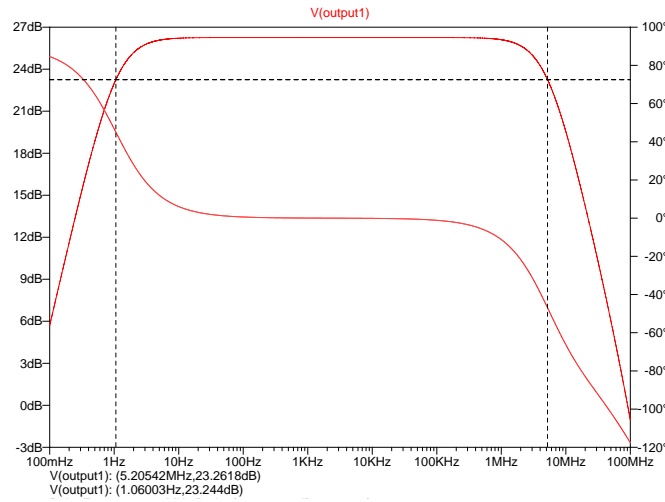


Figure 4.21: LT Spice AC sweep simulation result for *Amp 1* in figure4.19

The final LNA output (output at *Amp 3*) is shown in figure 4.22. Typical third order bandpass filter characteristics (60 dB per decade) are noted from amplitude response. The maximum gain of the LNA is 78.7961 dB. The effect of the three high pass filters *HPF 1*, *HPF 2* and *HPF3* in figure 4.19 combine to give the -3 dB high pass cutoff frequency of 2.06 Hz. This is acceptable since it is below the 11 Hz bandwidth measured of the PLL in section 4.3.6. The combined -3 dB low pass cutoff frequency caused by the feedback capacitors C_1 , C_2 , and C_3 is seen from figure 4.22 to be 2.73 MHz. This satisfactory since it is larger than the 1 MHz specified in section 4.4. As more of the amplifier stages are included in the LNA, the bandwidth becomes smaller. Table 4.2 shows the LNA bands depending on how many amplifier stages are included in the LNA.

Table 4.2: Different -3 dB cutoff frequencies of the LNA depending on how many of the amplifier stages are included.

	Amp 1	Amp 2	Amp 3
-3 dB low pass cutoff frequency	5.21 MHz	3.42 MHz	2.73 MHz

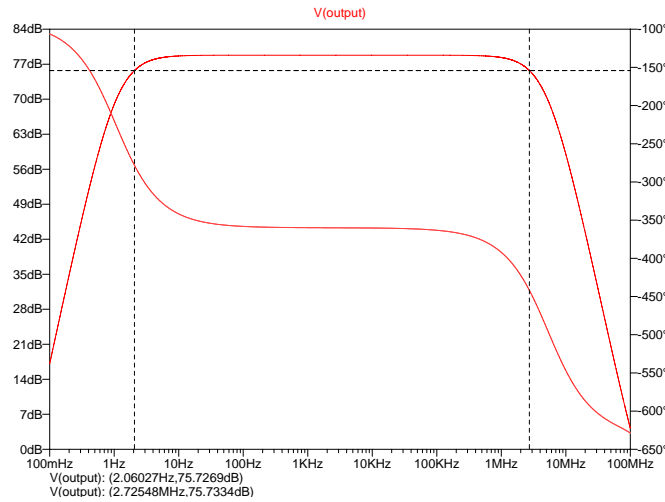


Figure 4.22: LNA LT Spice AC sweep simulation results, measured at the output of *Amp 3*

4.5.4 Measurement

To measure the LNA amplitude response a 0 dBV signal is generated and then attenuated by 80 dB before connecting it to the LNA. The measurement setup is shown in figure 4.23.

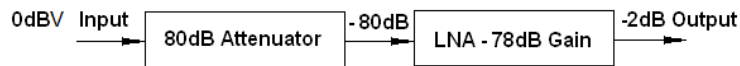


Figure 4.23: Measurement setup for the LNA frequency amplitude response

Attenuating the test signal 80 dB prevents the LNA from being saturated with large signals. The signal is swept over the different frequencies while the amplitude is kept constant. The amplitude response of the the output in figure 4.23 is measured with an oscilloscope. 80 dB is added mathematically to the measurement to compensate for the previous attenuation. The results are plotted in figure 4.24. The -3 dB low pass cutoff frequency is measured at 2.95 MHz and the -3 dB high pass frequency is measured at 5.8 Hz . The low pass cutoff frequency is close enough to the simulated value of 2.73 MHz . The high pass cutoff frequency is also close enough to the simulated 2.06 Hz .

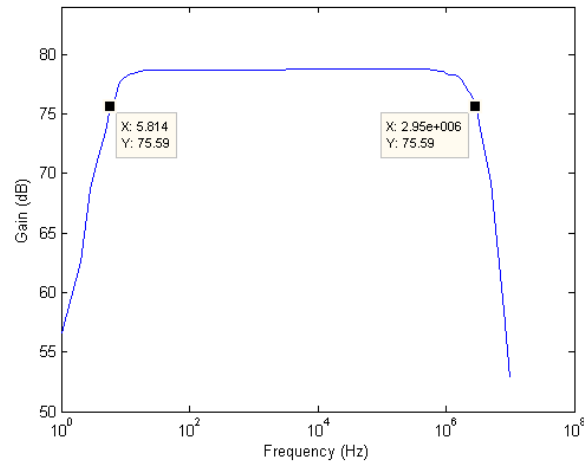


Figure 4.24: LNA amplitude response measurement.

4.5.5 Conclusion

The LNA is successfully designed, simulated and constructed. The final bandwidth measured for the LNA while all three amplifiers are included is $5,814\text{ Hz}$ to 2.95 MHz , as seen from figure 4.24. The phase noise band of interest in this thesis is between 10 Hz to 1 MHz . This means that there is an extra $2.95\text{ MHz} - 1\text{ MHz} = 1.95\text{ MHz}$ band of noise included in the output of the LNA. To further limit the output noise of the LNA, a 1 MHz low pass filter is needed at the LNA output. The LNA output filter is discussed in section 4.6. The maximum gain of the LNA when all three amplifiers are included is measured at 78.74 dB .

4.6 LNA Output LPF

The output bandwidth of the LNA of section 4.5 is measured at 2.95 MHz (figure 4.24). To further limit the LNA output band a low pass filter with -3 dB cutoff frequency of 1 MHz is needed. Usually this could be done by further limiting the feedback bandwidth of the operational amplifiers in figure 4.19. To support a modular design it is decided to design a separate low pass filter to perform this function. In the event that the LNA bandwidth needs to be increased, the LNA output LPF can be modified. Designing the LNA Output LPF further creates the opportunity to increase the order of the LNA output filter, since the combined low pass effect of the feedback capacitors C_1 , C_2 and C_3 are only equivalent to that of a third order filter. A fifth order LPF is required in order to suppress aliasing by at least 40 dB .

The filter design used for the LNA output LPF, is identical to the LNA Prefilter designed in section 4.4 and is included in the schematics in Addendum A.

4.7 ADC Prefilters

4.7.1 Introduction

Data is captured with the Tektronix TDS 1002B digital oscilloscope. The oscilloscope has a 60 MHz, 1 GS/s analog to digital converter (ADC) at both input channels. As discussed in section 5.2, the oscilloscope can only store 2500 data points per measurement. To increase the resolution of the phase noise measurements at low frequencies, the initial 10 MHz band from section 4.2 is split into three separate bands:

- Band 1: 10 Hz - 1 kHz
- Band 2: 1 kHz - 100 kHz
- Band 3: 100 kHz - 10 MHz

Consider Band 1: In order to measure the lowest frequency of 10 Hz a measuring time of at least 0.1 s is needed. To measure the highest frequency of 1 kHz within this band a Nyquist sampling speed of 2 kS/s is needed. A factor of 2.5 for the Nyquist frequency gives a sampling speed of 5 kS/s, which allows for a total measuring time of 0.5 s before the 2500 data point buffer is filled. The minimum frequency measurable under these conditions is $\frac{1}{0.5 s} = 2 Hz$, which in this case becomes the resolution of Band 1.

The parameters for Bands 2 and 3 are calculated similarly. Table 4.3 shows the three bands along with their resolutions, sample periods and corresponding sampling speeds.

Table 4.3: ADC Prefilter bands

	Bandwidth	Sampling frequency	Resolution	Sample period	Samples
Band 1	10 Hz- 1 kHz	5 ks/s	2 Hz	500 ms	2500
Band 2	1 kHz- 100 kHz	500 ks/s	200 Hz	5 ms	2500
Band 3	100 kHz- 10 MHz	50 Ms/s	20 kHz	50 μ s	2500

It can be seen from table 4.3 that the bandwidth of Band 2 is roughly 100 times larger than that of Band 1. Therefore the noise voltage that will be included in the measurement of Band 2 is 100 times larger than that of Band 1. To ensure that the ADC has the same number of bits in the noise floor when measuring Band 1 and 2, a gain of $10 \log 100 = 20 dB$ is needed when the

band becomes 100 times smaller. This is equivalent to a voltage gain of 10. The same argument is followed between Band 2 and 3.

The splitting of the bands along with the 20 dB gain is accomplished by active filtering. Figure 4.25 shows the setup of the filters:

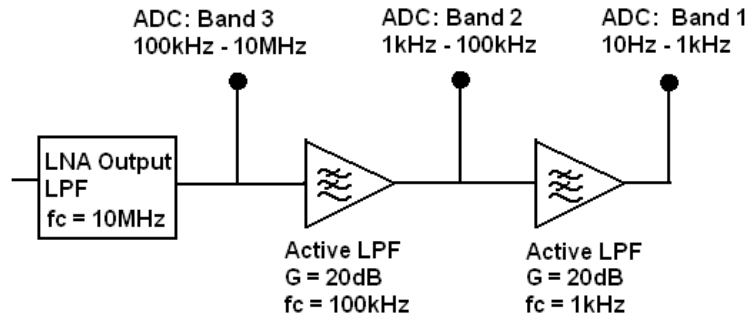


Figure 4.25: ADC Prefilters

4.7.2 ADC Prefilters Design & Simulation

The circuit diagram of the ADC Prefilters is shown in figure 4.26. The LNA Output LPF is followed by a DC block and a buffer. The DC block consists out of C_1 and R_1 which gives a -3 dB cutoff frequency of 1.06 Hz. It ensures that the ADC active Prefilters are not saturated by a DC voltage. The buffer prevents the LNA Output LPF from being loaded by the ADC Prefilters. In figure 4.26 the first active LPF lies between the nodes labeled *Band 3* and *Band 2*. The second active LPF is situated between the nodes labeled *Band 2* and *Band 1*. The active filters are designed with Filter Pro V2.0 from Texas Instruments. An AC analysis is performed on the circuit in LT Spice. The nodes labeled *Band 3*, *2* and *1* are measured and plotted in figure 4.27.

The bandwidths and gains of the ADC Prefilters are given in table 4.4.

Table 4.4: ADC Prefilter Bandwidths

	Band 3	Band 2	Band 1
-3 dB Cutoff frequency	1.19 kHz	118 kHz	9.41 MHz
Measured gain at area of flat amplitude response	38.47 dB	19.23 dB	0 dB

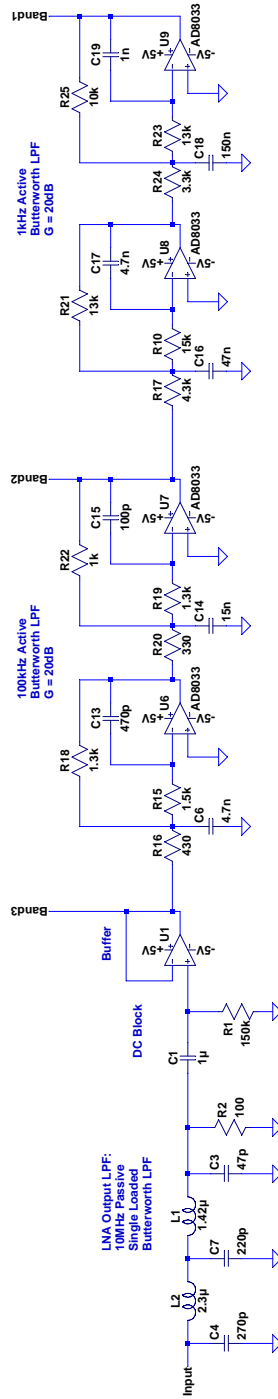


Figure 4.26: ADC Prefilters circuit diagram

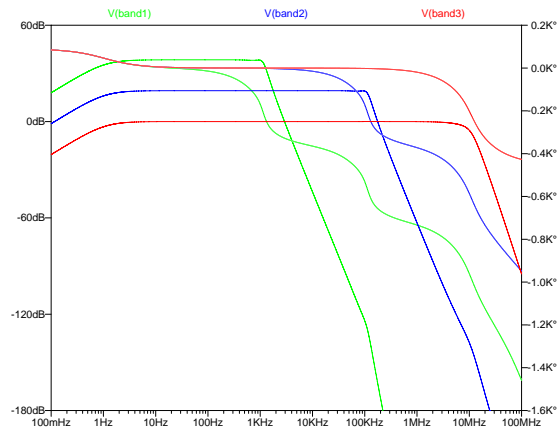


Figure 4.27: LT Spice simulation of ADC Prefilters bandwidths

4.7.3 Measurements

The filter described in figure 4.26 is constructed. The amplitude responses of the active filters are measured by applying a frequency sweep at the node labeled INPUT in figure 4.26 and measuring nodes labeled *Band 1*, *2* and *3*. Since the active filters have gains of almost 20 dB , the amplitude of the frequency sweep needs to remain small enough so that the active filters do not become saturated. The test signal amplitudes and -3 dB bandwidths of the ADC Prefilters are listed in table 4.5 and the measurements are illustrated in figure 4.28. The LNA output filter -3 dB bandwidth is also listed in this table. The measured gains and bandwidths for each of the bands are within 10% of the simulated values.

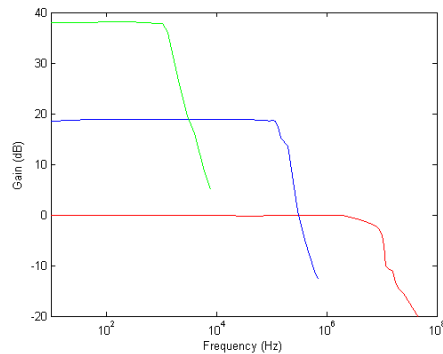


Figure 4.28: ADC Prefilter amplitude response measurement

Table 4.5: ADC Prefilter bandwidth and gain measurements

	Band 1	Band 2	Band 3
Test signal amplitude applied at node labeled <i>Input</i>	0 dB	-20 dB	-40 dB
-3dB Cutoff frequency	9,01 MHz	145 kHz	1,33 kHz
Measured gain at area of flat amplitude response	-0.12 dB	18.8 dB	38.8 dB

4.7.4 Conclusion

From table 4.5 the bandwidth of the ADC Prefilters are noted to be larger than the simulated values in both cases for Band 2 and Band 3. Since these two filters have very steep filter decay gradients (fourth order), the somewhat higher filter cutoff frequencies are acceptable.

4.8 Conclusion

This chapter contains a discussion on the successful design, simulation and measurement of all the hardware components which facilitate the phase demodulation. A modular approach is taken in designing the phase noise measuring system by dividing the design into modular components. Doing so creates the opportunity for hardware component interchangeability. Should the measurement of phase noise be required that is outside the limits of the current design, only certain hardware components can be replaced.

In section 4.3 the designed PLL bandwidth is measured as 11 Hz.

Section 4.4 discuss the LNA Prefilter which strips $e_o(t)$ from the sum frequency component and limits the input bandwidth to the LNA to 1.02 MHz. The LNA is passive to minimize its noise contributions.

A variable gain LNA, with a maximum gain measured at 78.74 dB, is developed in section 4.5. The LNA amplifies the measured phase noise until it is large enough to be sampled.

The output of the LNA is band limited to 1 MHz by the LNA Output LPF developed in section 4.6.

ADC Prefilters developed in section 4.7 splits the initial phase noise measuring bandwidth of 10 Hz - 10 MHz in three bands; 10 Hz - 1 kHz, 1 kHz - 100 kHz and 100 kHz - 10 MHz. Doing so increases the frequency resolution of the measured phase noise in the lower bands.

Chapter 5

Data Acquisition & Digital Signal Processing

5.1 Introduction

The phase noise measured by the hardware developed in Chapter 4 needs to be digitized and Fast Fourier transformed (FFT). The measured phase noise can then be displayed as one-sided, single sideband phase noise $\mathcal{L}(f)$ as in figure 2.7b.

This chapter entails the means by which the measured phase noise is converted from analog signals to digital samples. An FFT analysis is performed on the samples provided by the ADC. The FFT noise floor is explained as well as the affect it has on the dynamic range or the phase noise measuring system. The effects of windowing are also explained with examples.

5.2 ADC - Tektronix TDS 1002B

Taking time, money and effort into consideration the Tektronix TDS 1002B Digital Storage Oscilloscope from National Instruments [12] is incorporated for data acquisition. It has a 2-channel, 8-bit ADC with a sampling speed of up to 1 GS/s and a bandwidth of 60 MHz . The maximum sample storage length is 2500 samples. The oscilloscope has a variable input gain that allows its ADC full scale value to be adjusted between 40 V and 16 mV . All measured data is sent via USB to a desktop computer with Matlab R2007a for post processing. This oscilloscope is the N -bit ADC and M -word buffer as seen in figure 5.2, with $N = 8$ and $M = 2500$. Figure 5.1 shows a front view of the Tektronix oscilloscope.

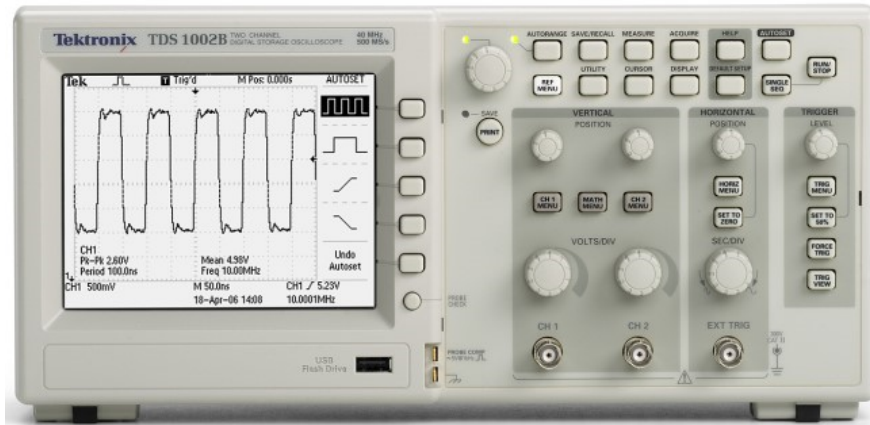


Figure 5.1: Tektronix TDS 1002B Digital Storage Oscilloscope

5.3 FFT Analysis of ADC output

5.3.1 Test Setup for FFT analysis of ADC output

Figure 5.2 shows the setup for an FFT analysis of an ADC output.

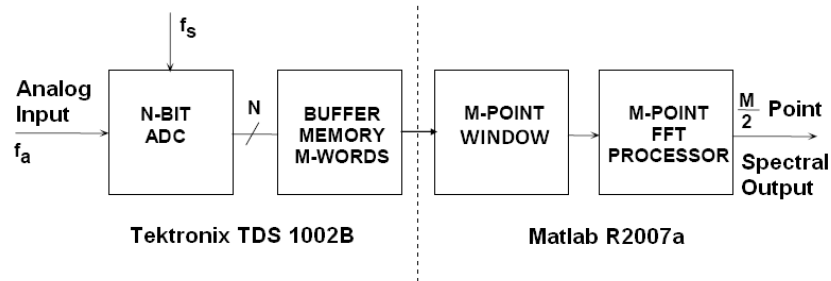


Figure 5.2: Test Setup for FFT Analysis of ADC Output

The analog input is sampled by the N -bit ADC at a sampling frequency of f_s and stored in the M -word buffer, both of which are done with the Tektronix oscilloscope. M is the length of the FFT which is the number of samples stored in buffer. The M -word buffer content is forwarded via USB to Matlab R2007a on a desktop PC in which a M -point time domain window is applied to the sampled data. Applying different windows has the desired effect of suppressing the side-lobes (caused by the default square window) of single frequency components making

small frequency components that are close to the large frequency component visible. This comes at a price as the main lobe becomes wider. It also costs “gain”. In figure 5.3 square, Hanning, and ChebyChev windows are individually applied to a sampled signal. The signal is composed out of a $1 V_{rms}$ $300 Hz$ component, a $2 mV_{rms}$ $350 Hz$ component and white noise. The figure illustrates the effect of different window types on the thickness of the main lobe and side lobes. Note that the single frequency components and the white noise are each lowered by different amounts, depending on which window is used.

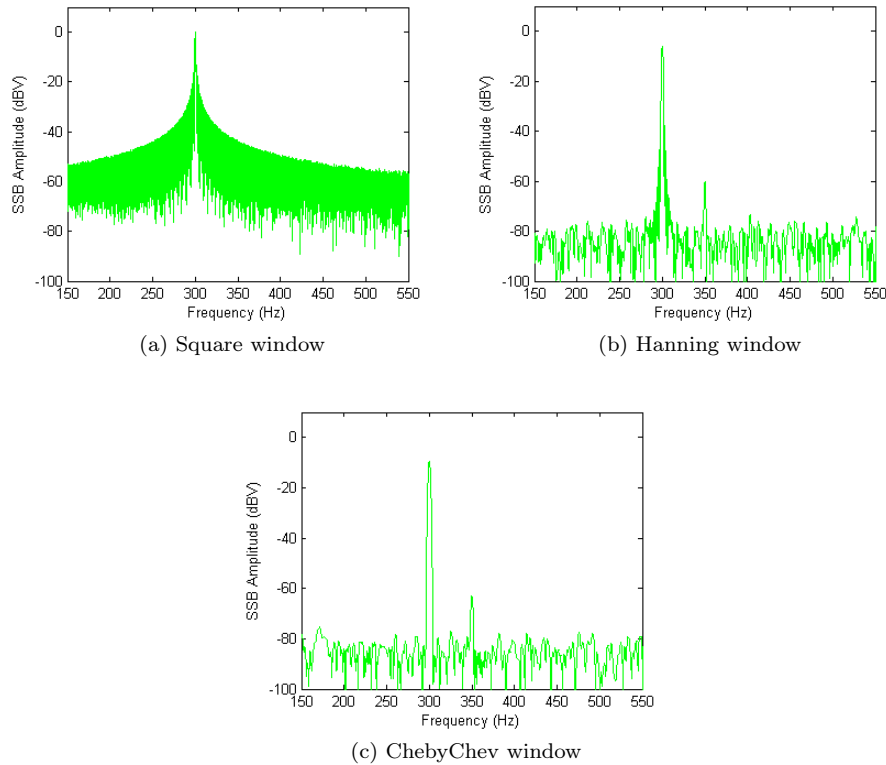


Figure 5.3: Square, Hanning and ChebyChev windows are individually applied to a sampled signal that is composed out of a $1 V_{rms}$ $300 Hz$ component, a $2 mV_{rms}$ $350 Hz$ component and white noise.

The spectral output of the FFT in figure 5.2 is a series of $M/2$ vector points in the frequency domain. The spacing between the spectral output points is f_s/M . Due to the Nyquist theorem the total frequency range covered by the FFT in the spectral output is from DC to $f_s/2$. The resolution of the spectral output is f_s/M [13], which is also known as the *bin* size. An

improvement in resolution can be achieved by increasing the FFT length, M . From section 5.2, M is limited to 2500 in this thesis.

5.3.2 FFT Noise Floor

An example of a single-sideband (SSB) FFT output for the 8-Bit ADC of the Tektronix oscilloscope in section 5.2 is shown in figure 5.4. For this example the ADC full scale value was chosen at 400 mV. The quality of the output of the ADC is measured by the signal to quantization noise ratio (SQNR). SQNR is related to the number of bits N in equations 5.1 and 5.2 [13].

$$SQNR = \frac{3}{2} \cdot 2^{2N} \quad (5.1)$$

$$SQNR(dB) = 10 \log_{10} SQNR = 1.76 + 6.02N \quad (5.2)$$

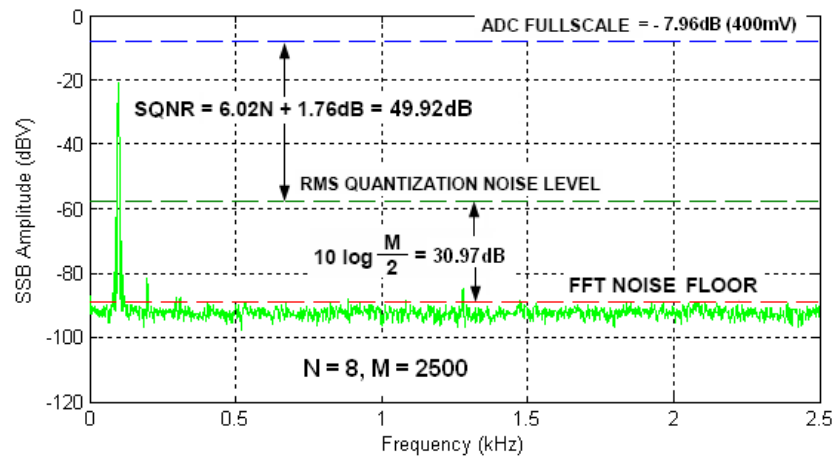


Figure 5.4: FFT Output for an 8-Bit ADC, Input = 100 kHz, $f_s = 5$ kSPS, Average of 5 FFTs, $M = 2500$

The SQNR results in the RMS quantization noise level as seen in figure 5.4. This level is at an offset from the ADC full scale value (the largest signal measurable by the ADC). The theoretical FFT noise floor is the sum of the RMS quantization noise level and that of the process gain $10 \log(M/2)$.

The value for the noise used in the calculation of SQNR extends over the entire Nyquist frequency range (DC to $f_s/2$), but the FFT acts as a narrow band spectrum analyzer with a

bandwidth of f_s/M that sweeps over the spectrum. Figure 5.5 illustrates this concept. The bandwidth f_s/M in (b) is larger than that of in (a) and will deliver larger values of noise measured since more of the noise is integrated into each bin. This is only true for power density spectrums (PDS's) such as Gaussian white noise. Consequently the process gain pushes the FFT noise floor down (which is the same as lowering the bandwidth on a spectrum analyzer) as seen in figure 5.4.

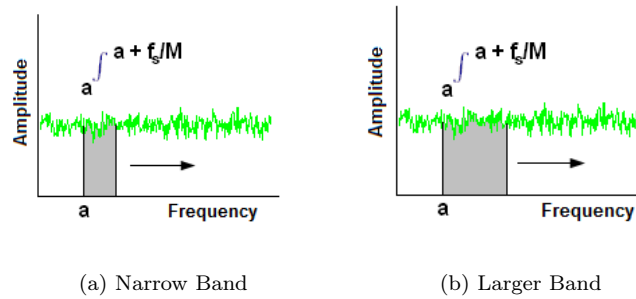


Figure 5.5: FFT Narrow band Spectrum Analyzer

5.4 Conclusion

This chapter discusses the FFT process from where the phase noise is sampled up to the point where it is displayed as one-sided, single sideband phase noise $\mathcal{L}(f)$. The phase noise is ADC with the Tektronix TDS 1002B Digital Storage Oscilloscope from National Instruments in section 5.2.

It is shown in section 5.3.1 that sampling windows such as Hanning or ChebyChev windows can be used to decrease the side lobes which are caused by the default square window.

The FFT noise floor is shown in section 5.3.2 to be dependent on the number of bits in the ADC. It is also dependent on the length of the FFT (number of samples stored from one measurement). The FFT noise floor is used in section 6.4 to calculate the dynamic measuring range of the phase noise measuring system.

Chapter 6

Calibration of Measuring System

6.1 Introduction

Up to this point all the individual hardware components have been designed and characterized. What remains is the calibration of the measuring system as a whole. Calibration of the system includes effects such as mixer conversion losses and mismatch losses between then individual hardware components when they are connected to form the complete measuring system..

First it is proved that the measuring system provides linear amplification for various levels of input signal power. Then the accuracy of the phase noise measuring system is determined by using an angle modulated signal to simulate phase noise.

After calibration a phase noise measurement is taken of the Marconi signal generator with the calibrated measuring system. The measurement is compared with another phase noise measurement of the Marconi signal generator which is taken by a Rohde & Swartz FSUP8 phase noise measuring system.

Finally the measuring dynamic range of the complete phase noise measuring system is determined.

6.2 Gain linearity

An experiment is performed to determine the linearity of the system gain with regards to the input signal strength. By linearity is meant that the measuring system will amplify smaller signals by the same amount as larger signals. Figure 6.1 shows the setup where a 7 dBm 10 MHz signal is mixed with a amplitude varied 10.001 MHz signal. The resulting frequency of the two mixed signals after filtering (LNA Prefilter) is 1 kHz . The amplitude of the 10.001 MHz signal is swept between -60 dBV and -100 dBV and the output amplitude is measured at the

point labeled Band 1.

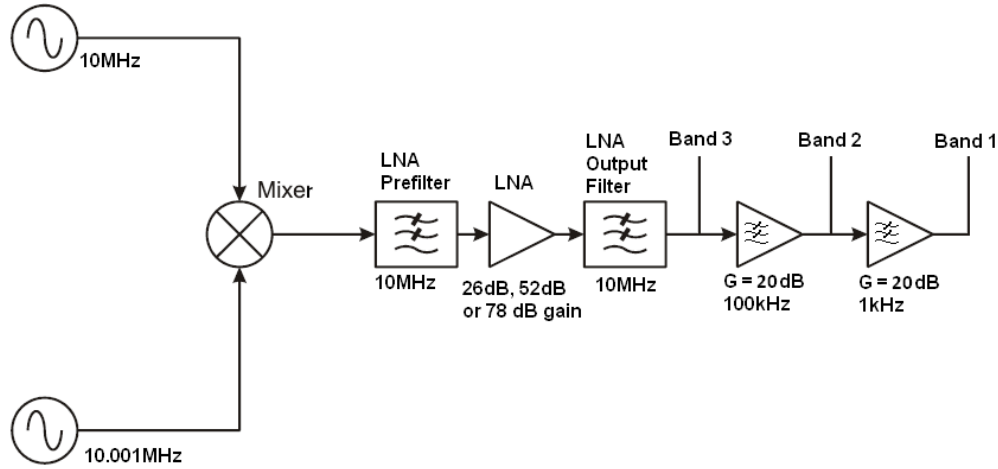


Figure 6.1: Amplitude linearity measurement setup

Table 6.1 shows the input signal amplitudes, output signal amplitudes and the measured gain.

Table 6.1: Amplitude linearity measurement results for Band 1

Input Amplitude	Output Amplitude	Gain = Output - Input
$1\text{ mV} = -60\text{ dBV}$	-3.328 dBV	56.67 dB
$100\text{ }\mu\text{V} = -80\text{ dBV}$	-23.44 dBV	56.56 dB
$10\text{ }\mu\text{V} = -100\text{ dBV}$	-43.15 dBV	56.85 dB

From table 6.1 the gain remains fairly constant with less than 0.3 dB variation for different input amplitudes. With the LNA set at 26 dB the rounded gain of 56.5 dB is the lowest gain of the measuring system.

Similar measurements are performed with the LNA set at 52 dB and 78 dB . The measured gain remains fairly constant with a variation off less than 0.3 dB . When the LNA is set at 78 dB the maximum gain of the measuring system in Band 1 is 112.5 dB .

Band 2 and 3 are also similarly tested for linearity and are found to also vary less than 0.3 dB .

The three different gains that each can be set for each band is summarized in table 6.2.

Table 6.2: The different gains for each of the Bands, depending on what the gain of the LNA is.

LNA gain	Minimum gain: 26 dB	Medium gain: 52 dB	Maximum gain: 78 dB
Measured Band 1 gain	56.5 dB	85.5 dB	112.5 dB
Measured Band 2 gain	36.5 dB	65.5 dB	92.5 dB
Measured Band 3 gain	16.5 dB	45.5 dB	72.5 dB

6.3 Phase Noise Measurement Calibration

Angle modulation theory is needed in order to understand how phase noise can be simulated. The following section gives a brief introduction to the special case of angle modulation - tone modulation.

6.3.1 Angle Modulation Theory

For the special case of tone modulation the modulation index β is defined as [14]

$$\beta = \frac{f_{\Delta}}{f_m} \quad (6.1)$$

where

- f_{Δ} - deviation of modulated signal in Hz
- f_m - modulation frequency in Hz.

Modulation index is the maximum value of phase deviation for both FM and PM. The angle modulated signal can be expressed in terms of its Bessel function components as discrete frequency components:

$$\hat{\phi}(t) = A \sum_{n=-\infty}^{\infty} J_n(\beta) \cos(f_c + n f_m) 2\pi t \quad (6.2)$$

where

- A - amplitude of carrier before modulation
- f_c - carrier frequency in Hz
- A - carrier amplitude in W
- $J_n(\beta)$ - Bessel function coefficient.

From equation 6.2 the modulated signal has a carrier component and an infinite number of sidebands frequencies $f_c \pm f_m, f_c \pm 2f_m, \dots, f_c \pm nf_m$. The higher the order of the sidebands (n), the smaller they become. Eventually the sidebands become small enough that they can be omitted [14] (less than 10% than the carrier). The size of β is used to determine the significant number of sidebands of the modulated signal, which is approximated by $n = \beta + 1$. This changes equation 6.2 as follow:

$$\hat{\phi}(t) = A \sum_{n=-(\beta+1)}^{\beta+1} J_n(\beta) \cos(2\pi f_c + n.2\pi f_m)t \quad (6.3)$$

The value for n is rounded to the nearest integer value. A table of Bessel functions can now be used in conjunction with equation 6.3 to determine the number and size (in power) of the significant sidebands. Figure 6.2 shows an example of a tone modulated signal where $\beta = A = 1$.

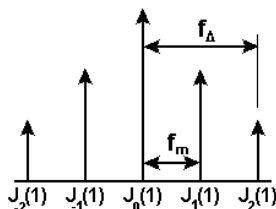


Figure 6.2: Carrier and significant sidebands of a tone modulated signal where $\beta = 1$.

6.3.2 Phase Noise Measurement Calibration

Narrow band FM is defined for when $\beta \leq 1$. In order to have only one significant sideband a β of 0.25 is chosen. From the table of Bessel functions the value of the coefficient $J_1(0.25)$ is read off as 0.124. Referred to the carrier it becomes $J_1(0.25) = 10 \log(0.124) = -9.066 \text{ dBc}$. By replacing the DUT of figure 4.1 with this narrow band FM signal, phase noise can be simulated at one specific frequency point as long as tone modulation is used. The frequency of the simulated phase noise at this point is the modulation frequency f_m . The amplitude of the simulated phase noise at this point is -9.066 dBc . The Marconi 2019A signal generator is used to generate this modulated signal. Figure 6.3 shows the phase noise measurement calibration setup.

When $f_m \leq 1 \text{ kHz}$, calibration measurements are taken at the point labeled Band 1.

When $1 \text{ kHz} < f_m \leq 100 \text{ kHz}$, calibrations measurements are taken at the point labeled Band 2.

When $f_m > 100 \text{ kHz}$, calibration measurements are taken at the point labeled Band 3.

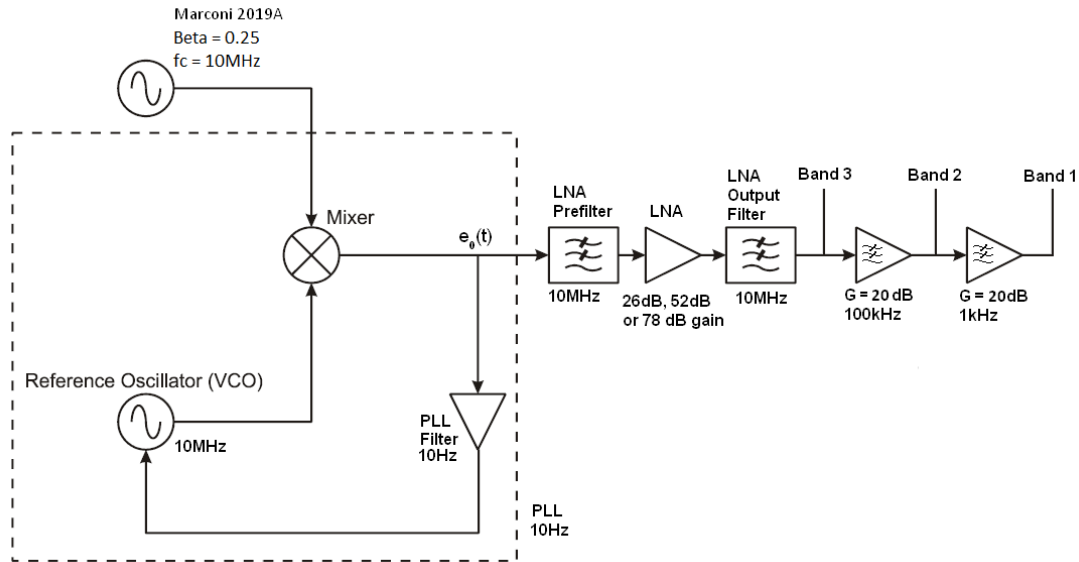


Figure 6.3: Phase noise measurement calibration setup performed by simulating phase noise with a narrow band FM modulated signal.

β is kept at a constant value of 0.25 so that the expected value of $J_1(\beta)$ remains -9.066 dBc as f_m is swept over a range of frequencies. $J_1(0.25)$ that is measured at each of those frequencies deviates from the expected -9.066 dBc due to the inaccuracy of the Marconi signal generator used in this calibration and due to the imperfections in the measuring system.

Figure 6.4 shows a single measurement of J_1 measured by the phase noise measuring system where $f_m = 976 \text{ Hz}$ and $\beta = 0.25$.

Figure 6.5 shows $J_1(0.25)$ that is measured by the phase noise measuring system over the frequency range of 40 Hz to 400 kHz . The output of the Marconi signal generator is continually measured by a spectrum analyzer and also plotted on figure 6.5 as the input $J_1(0.25)$. The expected value calculated for $J_1(0.25)$ is -9.066 dBc . This is also plotted on the figure to show that the input signal generated by the Marconi signal generator varies in amplitude.

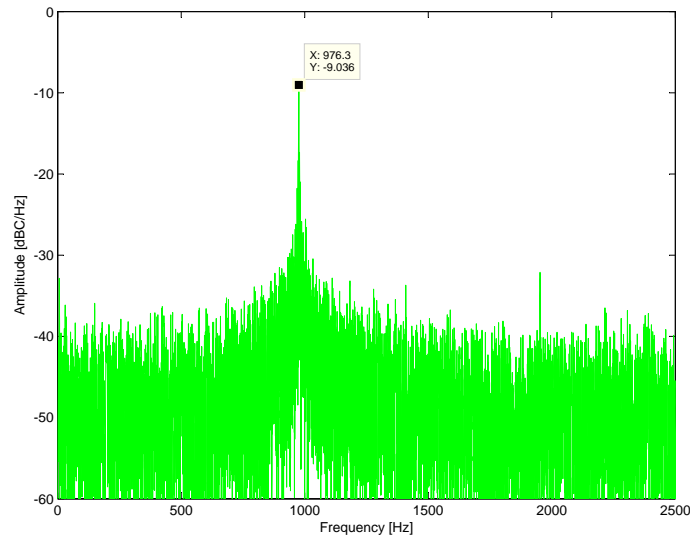


Figure 6.4: Phase noise simulation measurement of $J_1(0.25)$ where $f_m = 976.3 \text{ Hz}$.

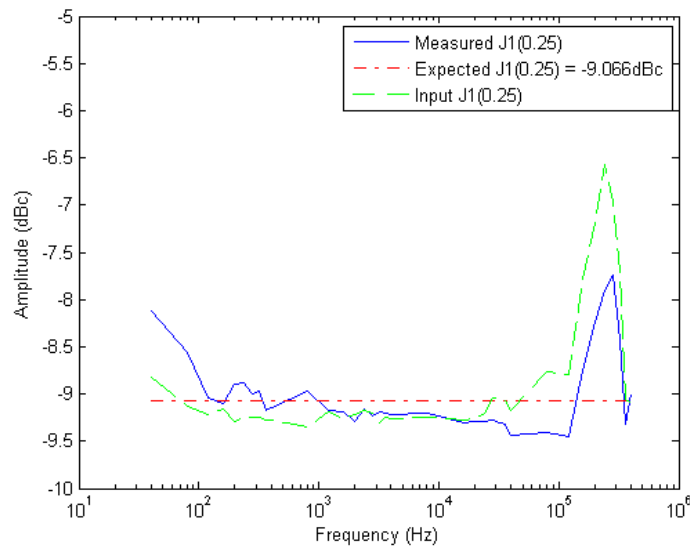


Figure 6.5: Measured values of $J_1(0.25)$ where f_m is swept over 40 Hz to 400 kHz

From figure 6.5 the values for $J_1(0.25)$ that are measured by the phase noise measuring system looks similar to the output of the the Macroni signal generator. The accuracy of the phase noise measuring system is determined from the figure by calculating the difference between the input signal and the measured signal. The largest error is made at $240kHz$ and is calculated as $1.2dB$. The error at their respective frequency positions are stored. When phase noise measurements are made, those errors are removed from the phase noise measured. (In order to aquire the value by which each frequency point must be calibrated, the points in figure 6.5 are interpolated.) Such a measurement is a calibrated measurement.

An example of a calibrated measurement taken by the measuring system developed in this thesis for Band 1 is compared to a measurement that is taken by a Rohde & Schwartz FSEA30 phase noise measuring instrument in figure 6.6. The effect of the $10Hz$ PLL bandwidth can be seen from the figure. The two measurements are very close to identical.

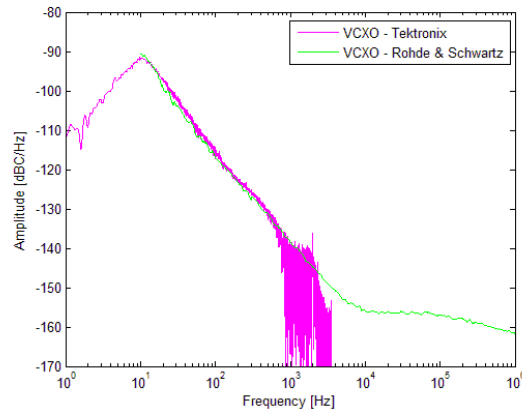


Figure 6.6: A calibrated phase noise measurement taken by the phase noise measuring system developed in this thesis is compared to a measurement that is taken by a Rohde & Schwartz FSEA30 phase noise measuring instrument.

6.4 Dynamic Range

6.4.1 Introduction

The dynamic range of the phase noise measuring system is defined as the ratio of the largest phase noise measurable to the smallest phase noise measurable. The factors that limit the maximum and minimum phase noise measurable are discussed. Finally the dynamic range of the phase noise measuring system is determined through measurements.

6.4.2 Maximum phase noise measurable

The maximum phase noise measurable is determined by two limits. The first limit is imposed when the carrier power becomes larger than what the mixer can safely operate with. The ADE-2 data sheet [8] give a maximum RF power of 17 dBm . Including a safety margin of 7 dB on the RF power limits the maximum carrier power to 10 dBm in this thesis.

The second limit is reached when the op-amps of the ADC Prefilter begin to saturate. This occurs when the phase noise $e_0(t)$, created by the phase detector as seen in figure 4.1, becomes too large. The first op-amp that saturates is the last one of the ADC Prefilter chain, which is in the $10\text{ Hz}-1\text{ kHz}$ bandwidth (Band 1) in figure 4.26. The AD8033 data sheet [15] gives a worse case maximum output voltage swing of $\pm 4.75\text{ V}$ when supplied with $\pm 5\text{ V}$. Adding a safety margin of 250 mV limits the maximum output voltage swing to $\pm 4.5\text{ V}$. Using the minimum gain of Band 1 in table 6.2, the maximum phase noise measurable is calculated as -43.44 dBV ¹. The maximum phase noise for Band 2 and 3 is calculated similarly. The maximum phase noise measurable by the measuring system for each of the three bands is listed in table 6.3.

Table 6.3: Maximum phase noise measurable in Band 1, Band 2 and Band 3

	Band 1	Band 2	Band 3
Maximum phase noise measurable	-43.44 dBV	-23.44 dBV	-3.44 dBV

The phase noise used here is the worst case scenario where the phase noise is a single frequency component. Usually phase noise is distributed as a voltage density spectrum and is much lower than that of a single frequency component. It is the peak value of the phase noise that will saturate the ADC Prefilter op-amps.

6.4.3 Minimum phase noise measurable

There are two factors that can limit the minimum phase noise measurable. It can either be limited by the FFT noise floor (figure 5.4) of the measuring system, or it can be limited by the thermal noise floor of the measuring system. The largest noise floor of these two noise floors is the minimum phase noise measurable.

¹The maximum phase error unit is not given here as $\text{dBc}/\sqrt{\text{Hz}}$. It is the peak size of the phase error that causes the op-amps to saturate, not the size of it referred to the carrier. The phase noise can for example be $-20\text{ dBc}/\text{Hz}$ and will still not cause the op-amps to saturate, provided that the carrier amplitude is less than 23 dBV .

Minimum phase noise measurable due to the FFT noise floor:

The minimum ADC full scale value of the Tektronix oscilloscope is 16 mV . Figure 5.4 shows that the minimum FFT noise floor can be calculated as follow:

$$\begin{aligned} FFT\ Noise\ floor_{min} &= 20\log(0.016) - 49.92\text{ dB} - 30.97\text{ dB} \\ &= -109.81\text{ dBV} \end{aligned} \quad (6.4)$$

Taking into account the maximum gain of each of the measuring bands from table 6.2 and the resolution of each Band from table 4.4, the minimum phase noise measurable due to the FFT noise floor is calculated as follow:

$$Noise\ Floor_{min} = -FFT\ Noise\ floor_{min} - gain_{max} - 20\log\sqrt{resolution} \quad [dBV/\sqrt{Hz}] \quad (6.5)$$

The resulting $Noise\ Floor_{min}$ for each of the 3 bands are displayed in table 6.4

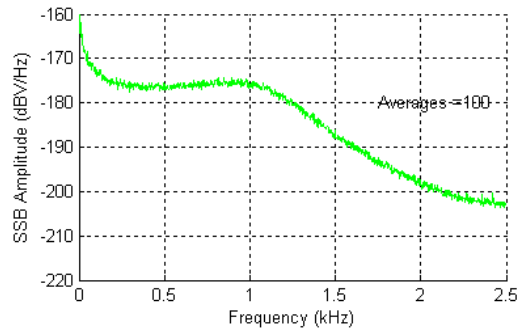
Table 6.4: Minimum phase noise measurable in each of the three Bands, due to the FFT noise floor

	Band 1	Band 2	Band 3
$Noise\ Floor_{min}$	$-225.32\text{ dBV}/\sqrt{Hz}$	$-225.32\text{ dBV}/\sqrt{Hz}$	$-225.32\text{ dBV}/\sqrt{Hz}$

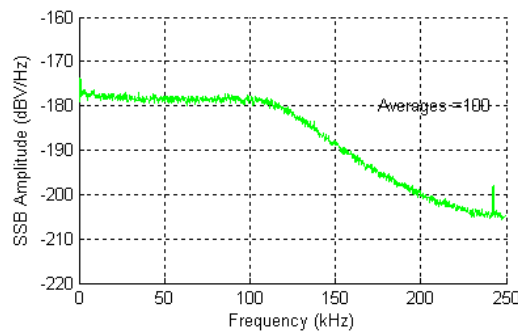
Minimum phase noise measurable due to the thermal noise floor:

Measuring the thermal noise floor of the phase noise measuring system hardware requires that the input of the LNA Prefilter in figure 4.1 be shorted to ground. Measurements are then taken at the nodes labeled Band 1, 2 and 3 in figure 6.3. The measured thermal noise floors for the different bands are illustrated in figure 6.7.

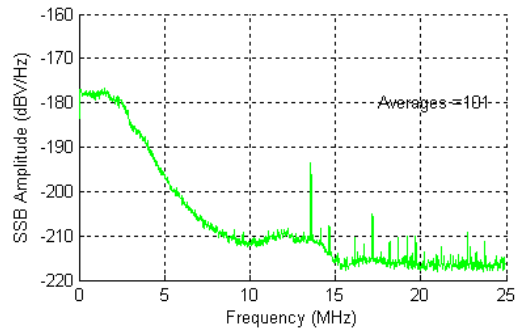
The minimum phase noise measurable due to the thermal noise floor is found to be approximately $-177\text{ dBV}/\sqrt{Hz}$ for each of the three Bands. This value is higher than the minimum phase noise measurable due to the FFT noise floor. Therefore $-177\text{ dBV}/\sqrt{Hz}$ is the minimum phase noise measurable by the phase noise measuring system, for all three of the measuring Bands.



(a) Band 1



(b) Band 2



(c) Band 3

Figure 6.7: Noise floor of the phase noise measuring system hardware

6.4.4 Conclusion

The dynamic range of the phase noise measuring system is determined by using the maximum values in table 6.3 and the minimum value measurable for phase noise which is $-177 \text{ dBV}/\sqrt{\text{Hz}}$.

The resulting dynamic ranges for the three Bands are listed in table 6.5.

Table 6.5: Dynamic range for Band 1, 2 and 3

	Min	Max	Total dynamic range
Band 1	$-177 \text{ dB}/\sqrt{\text{Hz}}$	-43.44 dB	133.56 dB
Band 2	$-177 \text{ dB}/\sqrt{\text{Hz}}$	-23.44 dB	153.56 dB
Band 3	$-177 \text{ dB}/\sqrt{\text{Hz}}$	-3.44 dB	173.56 dB

6.5 Conclusion

During this chapter the phase noise measuring system is calibrated. The gain linearity remains fairly constant with less than 0.3 dB variation for different input amplitudes. This remains true as long as the phase noise measured remains below the maximum value of -43.44 dB . The amplitude of the measured phase noise at any given frequency is determined to be accurate within 1.33 dB . Finally the dynamic ranges for each of the measuring bands is determined and listed in table 6.5.

Chapter 7

Crosscorrelation and Averaging

7.1 Introduction

Correlation is a mathematical operation which closely resembles convolution. Both cases involve two signal sequences. The mathematical result of correlation is, in contrast to convolution, a measure of the similarity between the two correlated signals. Correlation is used to extract information that is dependent on the application. It is often encountered in radar, sonar or digital communication applications. This chapter shows how the noise floor of the phase noise measuring system can be lowered by use of correlation and averaging. Correlation theory is introduced in section 7.2. A series of simulations are run in Matlab R2007a to test correlation and averaging. Finally the correlation and averaging is used practically in the phase noise measuring system to lower the noise floor.

7.2 Correlation Theory

Crosscorrelation¹ between the discrete time domain signals $x(n)$ and $y(n)$ is a sequence denoted $r_{xy}(l)$, which is defined as [16]

$$r_{xy}(l) = \sum_{n=-\infty}^{\infty} x(n)y(n-l), \quad l = 0, \pm 1, \pm 2, \dots \quad (7.1)$$

The subscripts xy on the crosscorrelation sequence $r_{xy}(l)$ is an indication of the sequences being correlated and the index l is the (time) shift parameter. The similarities between crosscorrelation and convolution of two sequences is apparent when looking at equation 7.1. With

¹Autocorrelation is the special case of crosscorrelation where $x(n) = y(n)$.

convolution one of the sequences are folded, shifted and multiplied by the other sequence to form the product sequence for that shift. Finally the values of the product sequence are summed. With crosscorrelation the same operations are involved, but without folding. Thus for crosscorrelation that leaves shifting, multiplying the two sequences and summing over all values of the product sequence. Equation 7.2 shows that if one of the sequences are folded, for example $y(-n)$, then convolution of $x(n)$ with $y(-n)$ yields crosscorrelation $r_{xy}(l)$:

$$r_{xy}(l) = x(l) * y(-l) \quad (7.2)$$

The Fourier transform of equation 7.2 gives

$$R_{XY}(s) = X(s) \times Y^*(s) \quad (7.3)$$

Therefor crosscorrelation can conveniently be performed by multiplying the Fourier transformed sequence $X(s)$ with the complex conjugate of the Fourier transformed sequence, $Y^*(s)$. The sequence $R_{XY}(s)$ is a frequency domain representation of the crosscorrelated sequence $r_{xy}(l)$ and is interpreted as a measure of similarity in frequency components between $x(n)$ and $y(n)$.

7.3 Correlation Simulations

7.3.1 Introduction

Simulations are run in Matlab R2007a to determine the effectiveness of crosscorrelation and averaging. The first simulation illustrates how the noise floor is lowered by crosscorrelation and averaging. The second simulation determines how much the measuring system noise floor is lowered by performing more crosscorrelations and averaging.

7.3.2 Simulation 1 - Lowering the noise floor

For the purpose of this simulation two composite signals are generated in Matlab. First, two cosines are defined:

$$s_1(t) = 0.1 \cos(2\pi 300t + \phi_1) \quad (7.4)$$

$$s_2(t) = 0.01 \cos(2\pi 800t + \phi_2) \quad (7.5)$$

where ϕ_1 and ϕ_2 are randomized initial phases. These cosines can be thought of as ideal single frequency components which are generated by a signal generator. Each time the signals are generated, they start off with random phases.

Signal $x(t)$ in equation 7.6 is composed out of the two cosines $s_1(t)$ and $s_2(t)$, as well as a Gaussian white noise component. Similarly, signal $y(t)$ in equation 7.7 is composed out of the same two cosines and also has a Gaussian white noise component.

$$x(t) = s_1(t) + s_2(t) + \text{whitenoise}_1(t) \quad (7.6)$$

$$y(t) = s_1(t) + s_2(t) + \text{whitenoise}_2(t) \quad (7.7)$$

The signals $x(t)$ and $y(t)$ is a representation of a composite signal, which has traveled through two different systems, each with unity gain. In figure 7.1 the two systems each add their own respective noise to the input and results in $x(t)$ and $y(t)$.

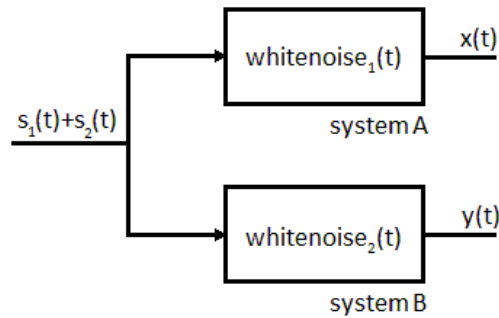
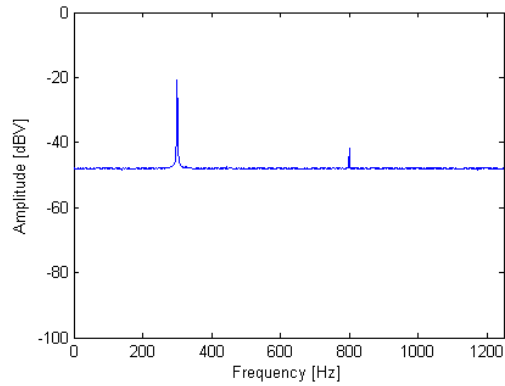
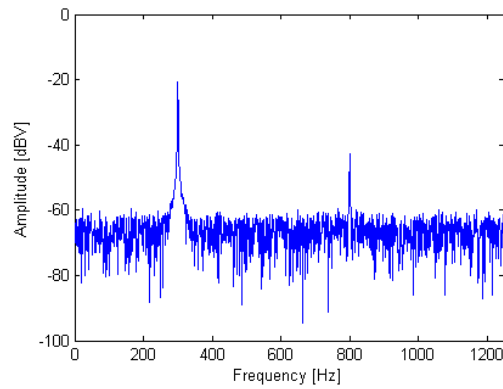


Figure 7.1: The individual noise from each system is added to the composite signal at the input to form $x(t)$ and $y(t)$.

A thousand measurements of the signal $x(t)$ are taken and the average of the Fourier transforms is shown in figure 7.2a. This is equivalent to making a measurement with a spectrum analyzer with an averaging set at 1000. Figure 7.2a shows $s_1(t)$ at 300 Hz, while $s_2(t)$ is barely visible at 800 Hz due to the high noise floor.



(a) Two frequency components with noise floor after only averaging.



(b) Two frequency components with noise floor after correlation and averaging.

Figure 7.2: The difference between correlation with averaging and only averaging.

Then the signals $x(t)$ and $y(t)$ are Fourier transformed and crosscorrelated using equation 7.3. The average of a thousand crosscorrelations R_{XY} is calculated with equation 7.8:

$$\overline{R_{XY}} = \frac{\sum_{n=1}^k R_{XY_n}}{k} \quad (7.8)$$

where $k = 1000$ for this case.

Figure 7.2b shows the resulting voltage density spectrum. Both $s_1(t)$ and $s_2(t)$ are now clearly visible above the noise floor at their respective frequencies of 300 Hz and 800 Hz. Calculating the average of a thousand crosscorrelations has lowered the noise floor by more than

10 dB. The composite signal $s_1(t)+s_2(t)$ is correlated in $x(t)$ and $y(t)$, resulting in the peaks at 300 Hz and 800 Hz. The white noise components in the signals $x(t)$ and $y(t)$, which was declared independently of each other, is mostly uncorrelated and results in the lower noise floor witnessed in figure 7.2b.

7.3.3 Simulation 2 - Improvement in noise floor with relation to number of averages

The purpose of this simulation is to determine how much the noise floor is lowered when the number of crosscorrelations is increased. Two independent signals of Gaussian white noise, $WHITENOISE_1(s)$ and $WHITENOISE_2(s)$ is generated. They are then correlated and averaged in the frequency domain for an increasing number of times.

After just one correlation the noise floor is lowered by 3 dB. An increase by a factor of ten in correlations and averaging corresponds to a lowering of the noise floor by an additional 5 dB. Figure 7.3 shows the relation between the number of times correlations were averaged and the improvement in noise floor.

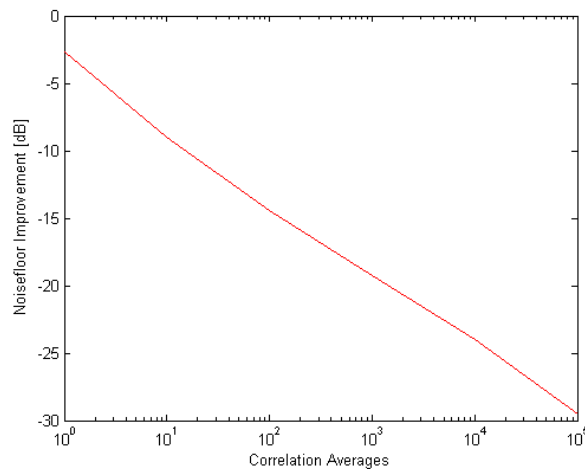


Figure 7.3: Improvement in noise floor when an average of more correlations are performed.

7.3.4 Conclusion

In this section it was proved that the noise floor can be lowered by means of crosscorrelation and averaging. The noise floor is dependent on the amount of crosscorrelations that are averaged.

For each increase in crosscorrelations by a factor of ten, the noise floor is pushed down by an additional 5 *dB*.

7.4 Correlation Measurements

7.4.1 Introduction

Two measurements are taken by using crosscorrelation and averaging. In Measurement 1 phase noise is simulated as have been done in section 6.3.2. It is shown that the noise floor is lowered without affecting the demodulated, simulated phase noise.

Measurement 2 shows that power spectral densities can also be correlated. Different resistor values are used and their correct power spectral densities are measured with crosscorrelation and averaging.

7.4.2 Measurement 1 - Crosscorrelation phase noise measurement

It is proved in section 7.3 that if a signal is passed through two different systems (figure 7.1), the noise of those two systems can be lowered by correlation and averaging. This is possible as long as the noise in the two systems is uncorrelated. The systems in figure 7.1 are each replaced by a phase noise measuring system from figure 4.1. The resulting crosscorrelation phase noise measuring system is shown in figure 7.1. Isolation transformers are placed at all the inputs of both Mixer_A and Mixer_B (not indicated on figure). This ensures that there are no ground loops that might cause oscillations.

Since the PLL of Measuring System A already ensures that the VCO is phase locked with the DUT, the PLL of Measuring System B is left disconnected. When a measurement is taken with the crosscorrelation phase noise measuring system, the noise due to mixers and individual Measuring Systems A and B, is uncorrelated, while the phase error $e_0(t)$ between the VCO and the DUT is correlated. It is therefore possible to take phase noise measurements that is lower than the noise floor of Measuring System A or B.

Just as in section 6.3.2, phase noise is simulated by use of a narrow band FM signal. The measurement setup is as seen in figure 7.4. The DUT is a 10 *MHz* signal with $\beta = 0.25$ and $f_m = 800$ *Hz*. A single discrete phase noise frequency $J_1(0.25)$ is thus expected at 800 *kHz*. Using the table of Bessel functions the expected amplitude is $10 \log(0.124) = -9.066$ *dBc*. The results from averaging 100 crosscorrelations is shown in figure 7.5.

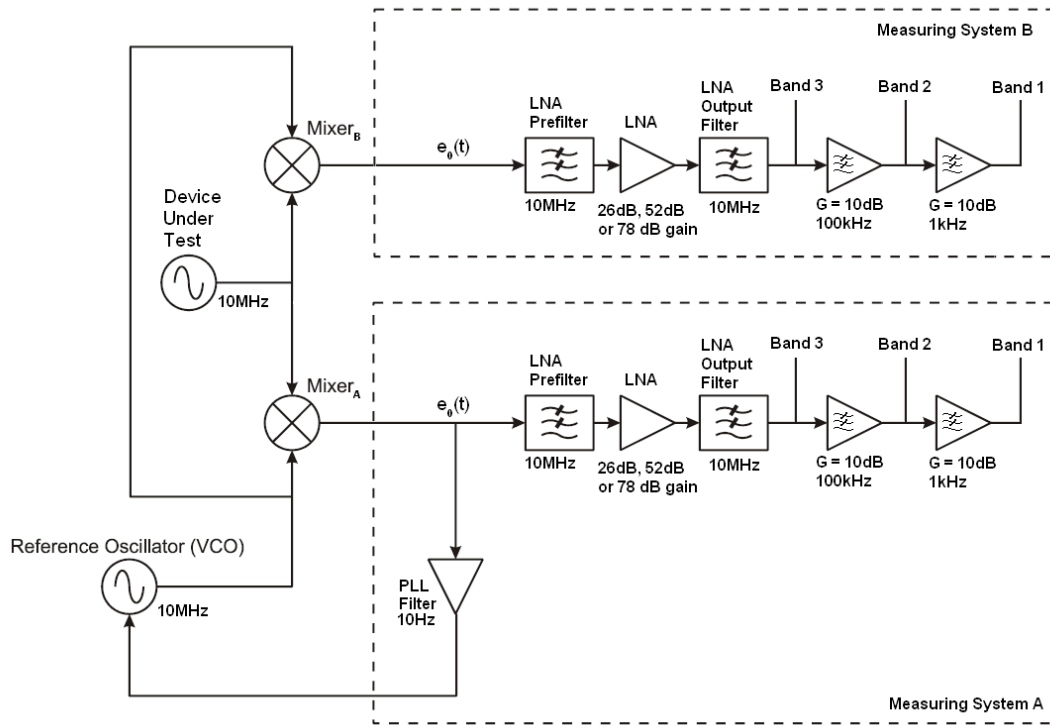


Figure 7.4: Crosscorrelation phase noise measuring system

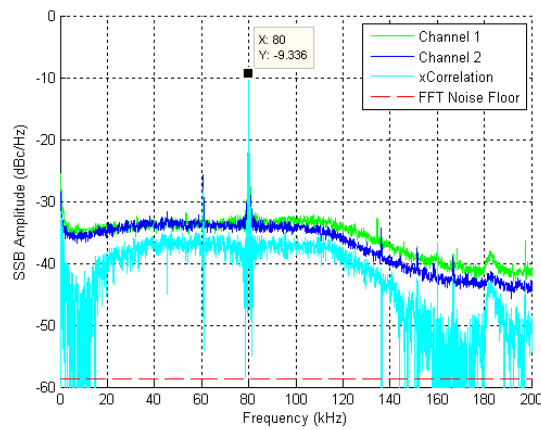


Figure 7.5: Average of 100 crosscorrelations of $J_1(0.25)$ where $f_m = 800 \text{ Hz}$

From figure 7.3 the correlated amplitude of $J_1(0.25)$ remains steady while the uncorrelated noise floor is reduced.

7.4.3 Measurement 2 - Voltage spectral density crosscorrelation measurement

To prove that crosscorrelation works as well on density spectra of phase noise as it does on discrete phase noise, crosscorrelated measurements of resistor thermal noise is taken. The thermal noise generated by resistors is given in equation 4.28. The measurement setup is shown in figure 7.6. The thermal noise voltage generated by the resistor is amplified by both Measuring System A and B. Each Measuring system adds their own noise. Measurements are taken at the nodes labeled Band 1, 2 and 3 in both Measuring System A and B. The measurements are repeated for the following resistor values: 220 Ω , 100 Ω , 47 Ω , 22 Ω , 10 Ω and 5.6 Ω . Figures 7.7, 7.8 and 7.9 illustrates the measured results. When the thermal noise voltage is larger than the noise floor of the measuring system, the average of crosscorrelations is the same amplitude of the noise floor. This is seen with all measurements taken with 220 Ω and 100 Ω resistors. When the thermal noise voltage becomes smaller than the noise floor of the measuring system, the average of crosscorrelations is smaller than the amplitude of the noise floor.

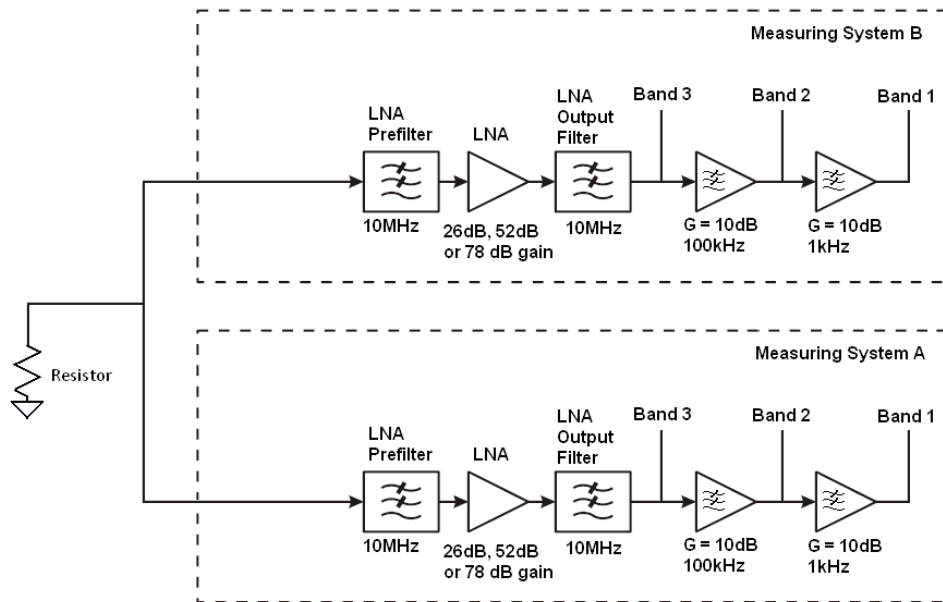


Figure 7.6: Voltage Spectral Density crosscorrelation measurement setup

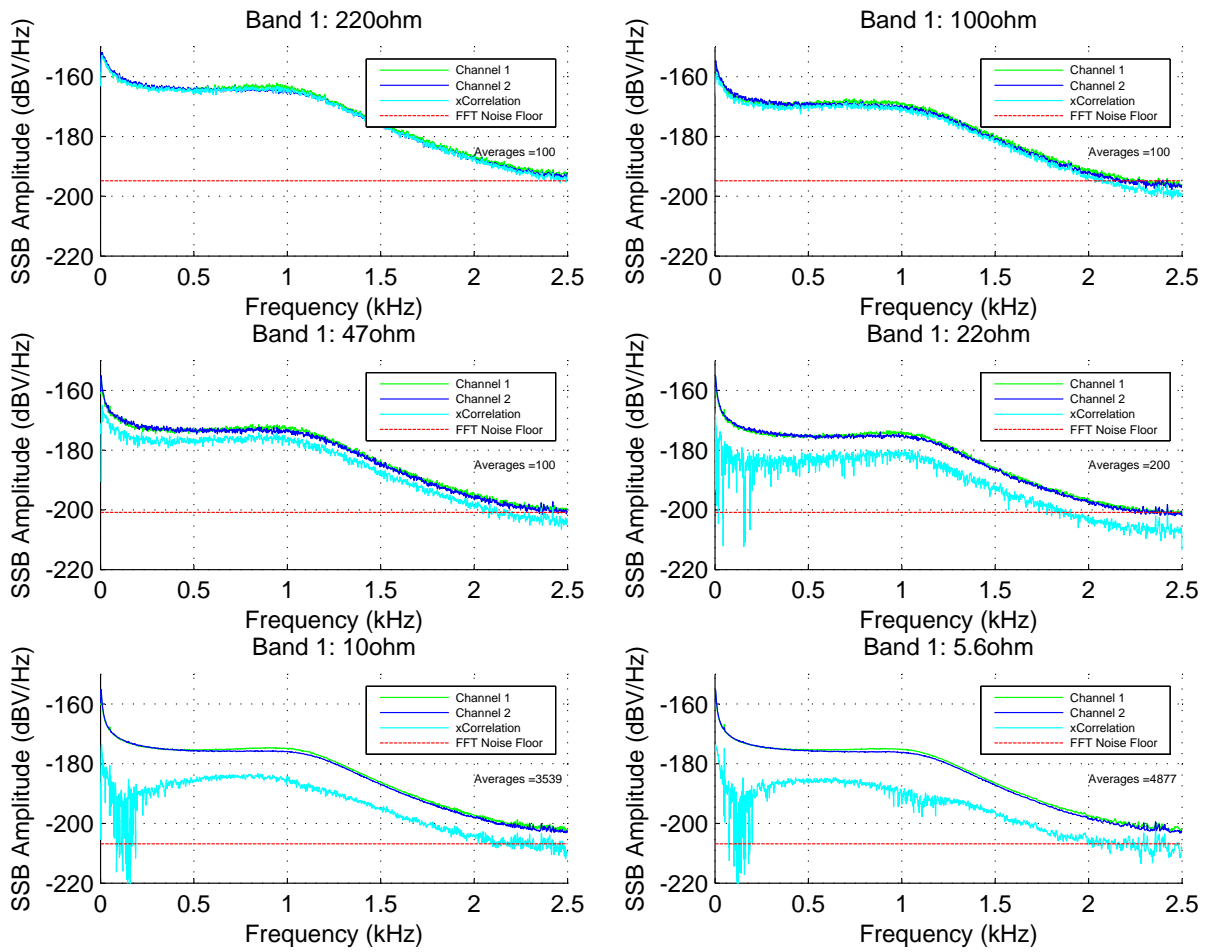


Figure 7.7: Band 1 voltage spectral densities of the thermal noise voltage generated by resistors of size $220\ \Omega$, $100\ \Omega$, $47\ \Omega$, $22\ \Omega$, $10\ \Omega$ and $5.6\ \Omega$.

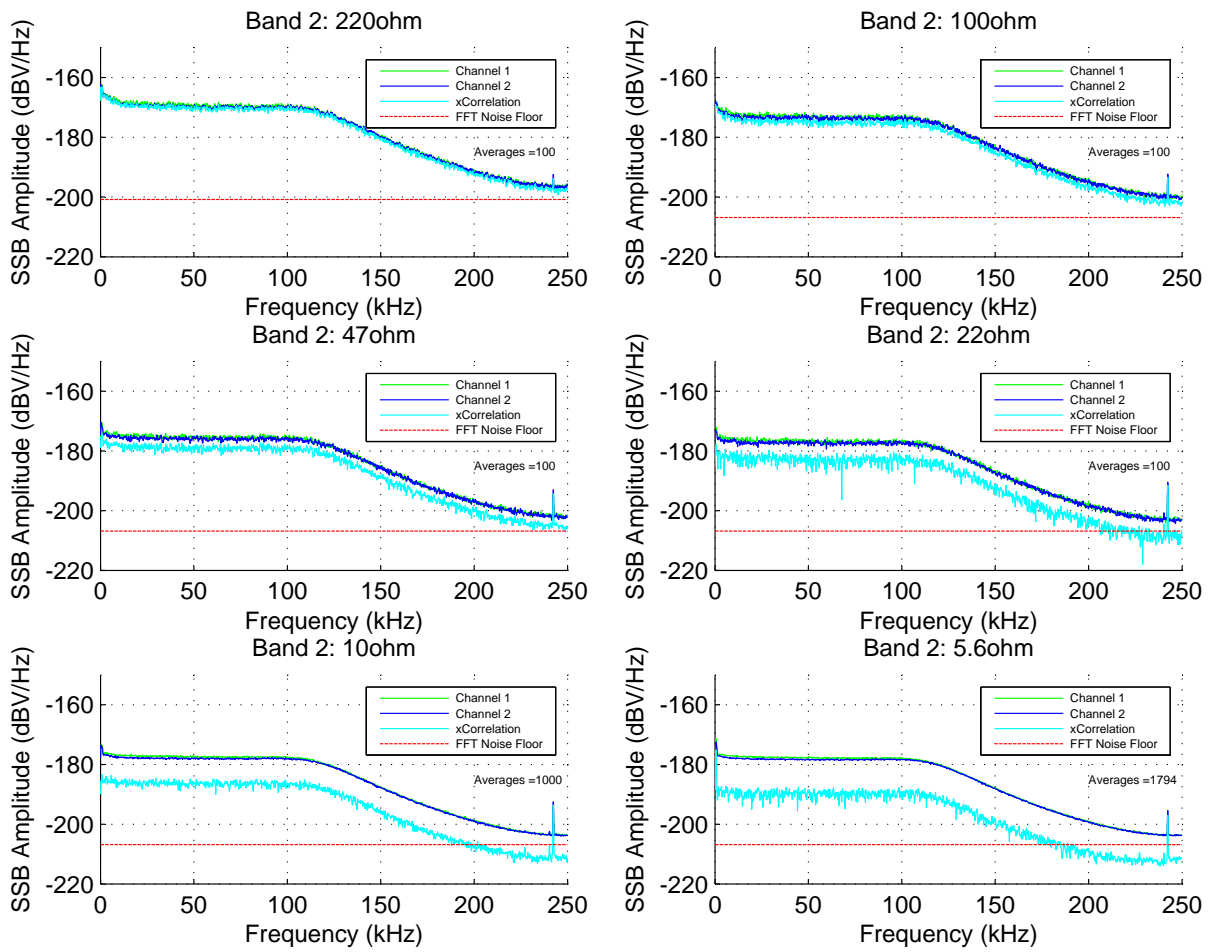


Figure 7.8: Band 2 voltage spectral densities of the thermal noise voltage generated by resistors of size 220 Ω , 100 Ω , 47 Ω , 22 Ω , 10 Ω and 5.6 Ω .

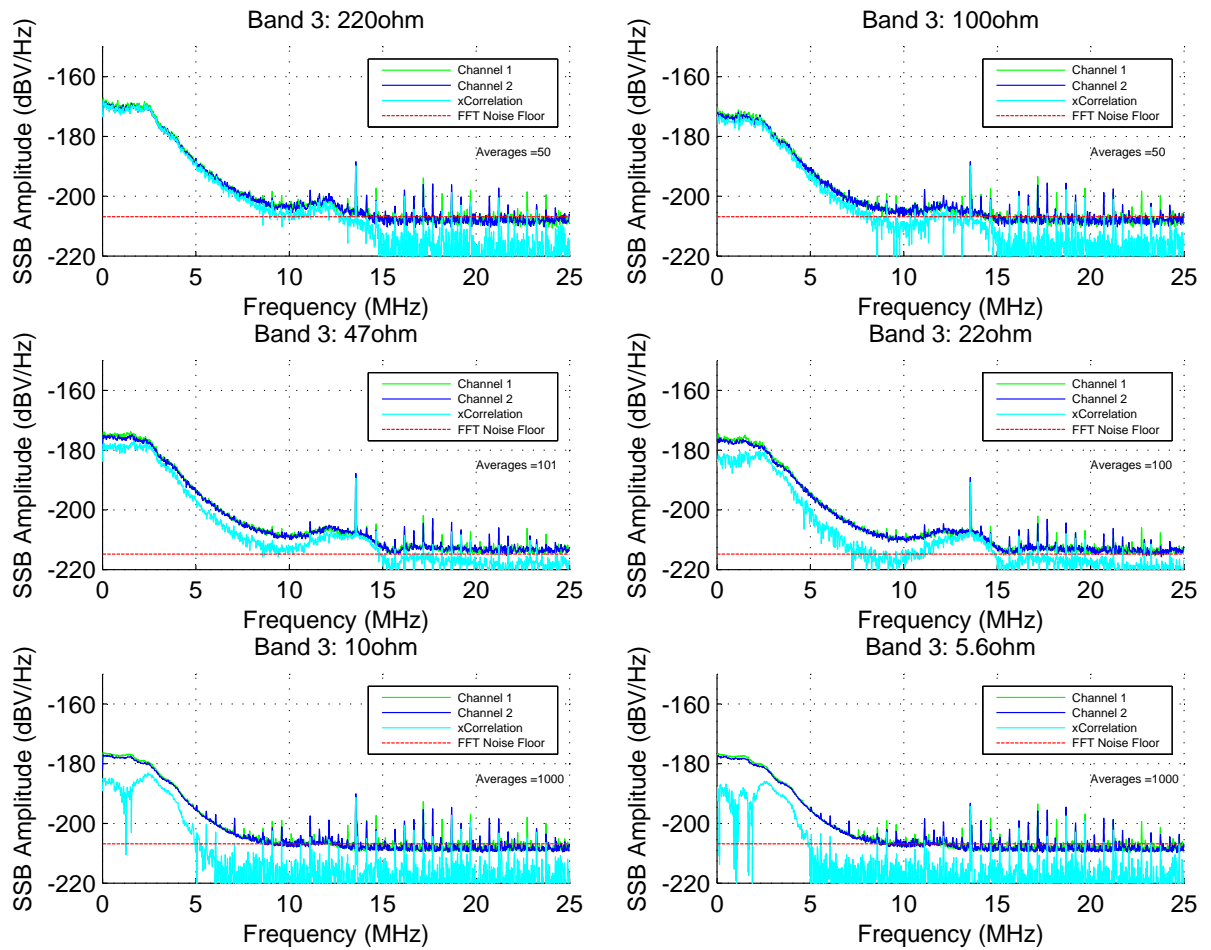


Figure 7.9: Band 3 voltage spectral densities of the thermal noise voltage generated by resistors of size 220 Ω , 100 Ω , 47 Ω , 22 Ω , 10 Ω and 5.6 Ω .

7.4.4 Conclusion

Crosscorrelation and averaging is effective in lowering the noise floor of the measuring system. Signals which are below the noise of the individual measuring system noise floors can still be measured, as long as those signals are correlated in both the measuring systems. Crosscorrelation and averaging is effective in both spurious a density spectra measurements.

7.5 Limits to Crosscorrelation and averaging

It was discovered experimentally that the average of crosscorrelations become inaccurate when it goes below the the FFT noise floor (defined in section 5.3.2). Therefor there is a limit to the crosscorrelation and averaging which lies at the FFT noise floor of each measurement. Further investigation is required to determine why the measurements become inaccurate when when averaging of crosscorrelation goes below the FFT noise floor.

The minimum phase noise measurable due to the FFT noise floor is given in table 6.4. The theoretical dynamic range of the phase noise measuring system, when crosscorrelation and averaging is used, is calculated with tables 6.3 and 6.4. The resulting theoretical dynamic ranges for each of the measuring bands when crosscorrelation and averaging is employed, is given in table7.1.

Table 7.1: Theoretical dynamic range of Band 1, 2 and 3 when crosscorrelation and averaging is used.

	Min	Max	Total dynamic range
Band 1	$-225.32 \text{ dB}/\sqrt{\text{Hz}}$	-43.44 dB	181.88 dB
Band 2	$-225.32 \text{ dB}/\sqrt{\text{Hz}}$	-23.44 dB	201.88 dB
Band 3	$-225.32 \text{ dB}/\sqrt{\text{Hz}}$	-3.44 dB	221.88 dB

7.6 Conclusion

The concept of crosscorrelation and averaging is introduced in this chapter. Simulations show that by using two separate measuring systems, the noise floor can be lowered through crosscorrelation and averaging. It is determined through simulation that the noise floor is lowered by and extra 5 dB for each increase in crosscorrelations by a factor of ten.

Crosscorrelation and averaging is then used practically in a phase noise simulation. The noise floor of the phase noise measuring system is reduced while the discrete measured phase noise amplitude remains the same.

Different resistor values, 220Ω , 100Ω , 47Ω , 22Ω , 10Ω and 5.6Ω are measured by using crosscorrelation and averaging to show that their respective voltage spectral densities can be determined, even if they are below the noise floor of the measuring system.

A limit to the crosscorrelation and averaging was found at the FFT noise floor. The improved dynamic ranges of Band 1, 2 and 3 due to crosscorrelation and averaging is shown in table 7.1.

Chapter 8

Conclusion

8.1 General Conclusion

In this thesis a phase noise measuring system that uses phase demodulation is successfully developed. It is shown that phase noise measurements as low as $-225.32 \text{ dB}/\sqrt{\text{Hz}}$ can be achieved by using crosscorrelation and averaging. Both spurious and continuous distributions of phase noise is accurately measurable within 1.2 dB of accuracy.

8.2 Recommendations

Some complications arose in the LNA as it would sometimes oscillate at 8.17 MHz . The hardware was constructed by use of a two layer PCB. It is theorized that oscillations arise due to ground loops. It is recommended that the hardware be constructed on a four layer PCB, where one whole layer is dedicated to ground and another layer to either positive or negative power.

The phase noise measurements performed by the measuring system developed in this thesis take a long time. The acquisition of data is limited by the communication speed between the Tektronix oscilloscope and the desktop computer. The measurement time can be significantly reduced by making use of a Freely Programmable Logic Array (FPGA) with 2 ADC connected to it. Post processing can than be performed on the FPGA at much greater speed than on the desktop PC.

A few aspects of the design can be modified in order to increase the dynamic range of the phase noise measuring system. Increasing the bit-rate and the FFT length (sample length) increases the FFT noise floor, and thus the dynamic range. A mixer with higher mixer gain can be used to increase the SNR of the measured phase noise, thereby also increasing the dynamic range.

Bibliography

- [1] R. Ziemer and W. Tranter, *Principles Of Communications: System Modulation And Noise*. Wiley-India, 2002. 1, 42
- [2] D. Pozar, *Microwave and RF design of wireless systems*, pp. 280–286. John Wiley & Sons, Inc. New York, NY, USA, 2001. 3, 7, 8
- [3] D. Howe, D. Allan, and J. Barnes, “Properties of oscillator signals and measurement methods,” *from the website of NIST as was found on*, vol. 10, 2005. 3, 15
- [4] E. Ferre-Pikal, J. Vig, J. Camparo, L. Cutler, L. Maleki, W. Riley, S. Stein, C. Thomas, F. Walls, and J. White, “Draft revision of IEEE STD 1139-1988 standard definitions of physical quantities for fundamental, frequency and time metrology-random instabilities,” in *Frequency Control Symposium, 1997., Proceedings of the 1997 IEEE International*, pp. 338–357, 1997. 3, 4, 5, 10, 11, 12
- [5] H. Packard, “Phase Noise Characterization of Microwave Oscillators,” *Product Note 11729B-1*. 12, 13
- [6] H. Packard, “Product note 11729b-1: Phase noise characterization of microwave oscillators - phase detector method,” publication date unavailable. 12
- [7] G. Nash, “Phase-locked loop design fundamentals,” *Motorola Inc. Phoenix AZ*, 1994. 27, 32, 33, 34
- [8] Mini-Circuits, “Datasheet: Surface mount frequency mixer - ade-2,” 2010. 29, 65
- [9] IQD-Frequency-Products, “Datasheet: Iqvcxo-161 leaded vcxo,” 2010. 31
- [10] K. Su and K. Su, *Analog filters*. Springer Netherlands, 2002. 39
- [11] Analog-Devices, “Datasheet: Ada4899-1,” 2010. 43
- [12] N. Instruments, “Datasheet: Tektronix tds 1002b digital storage oscilloscope,” 2010. 53

- [13] W. Kester, “MT-003: understand SINAD, ENOB, SNR, THD, THD+ N, and SFDR, so you don’t get lost in the noise floor,” <http://www.analog.com/en/content/0,2886,760%255F%255F91250,00.html/2005>, pp. 1–2. 55, 56
- [14] B. Lathi, *Modern digital and analog communication systems*. Oxford University Press, Inc. New York, NY, USA, 1998. 60, 61
- [15] Analog-Devices, “Datasheet: Ad8033,” 2010. 65
- [16] J. Proakis, D. Manolakis, D. Manolakis, and J. Proakis, *Digital signal processing: principles, algorithms, and applications*, vol. 4. Prentice Hall New Jersey, 2007. 69

Appendix A

Appendix A

A.1 PCB layout & EMI shielding

The complete circuit diagram is shown in figure A.1 and the PCB layout it shown in figure A.2. The circuit is lain out on a two layer, FR4 substrate. In order to counteract EMI two aluminum shields are soldered onto the PCB to cover the LNA and the LNA Prefilter. Doing so shields these sensitive areas from high frequency noise such as cell phone signals. The aluminum shields are labeled *Container1* and *Container2* in figure A.2a.

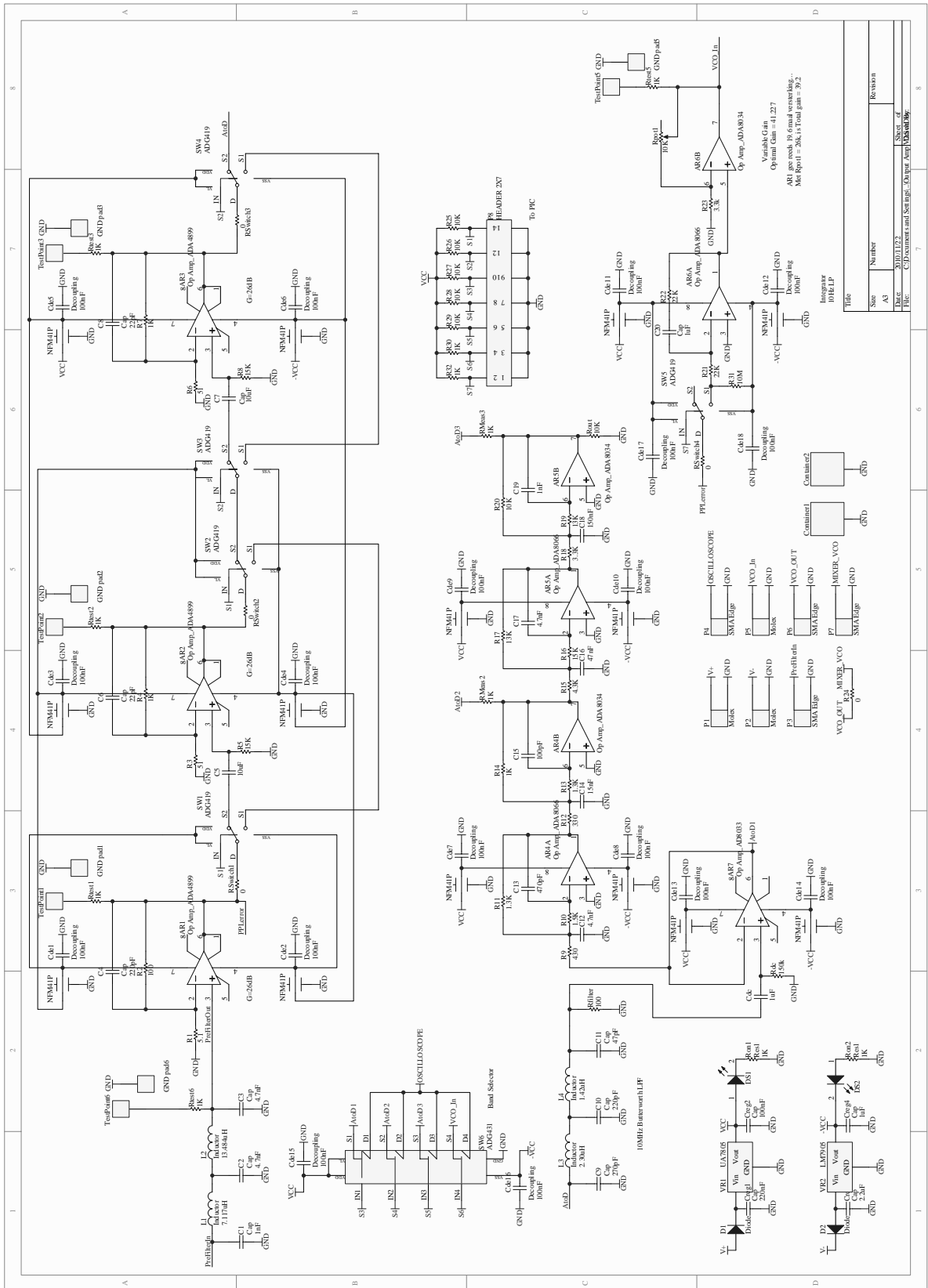
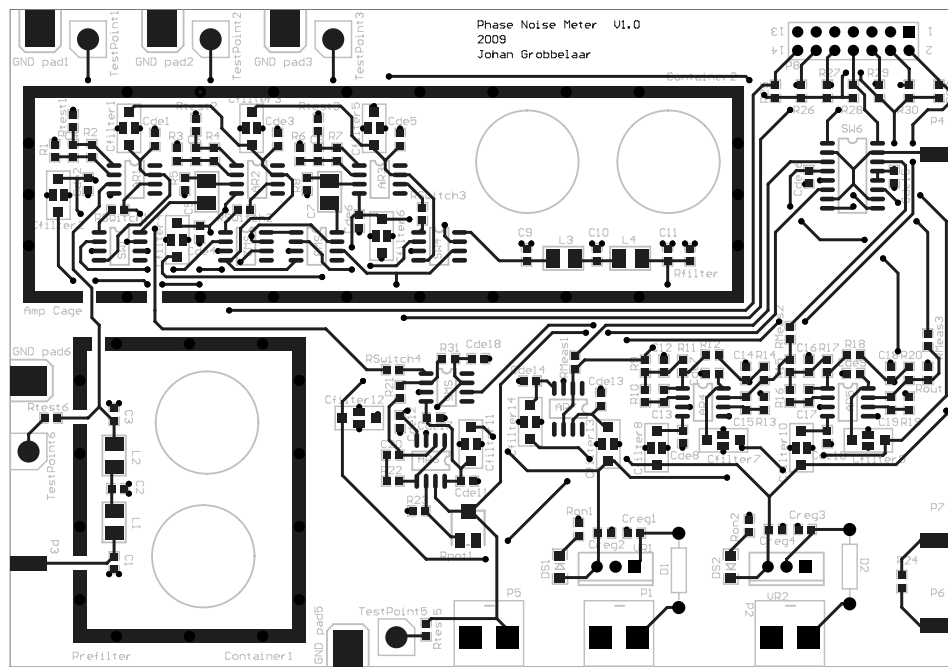
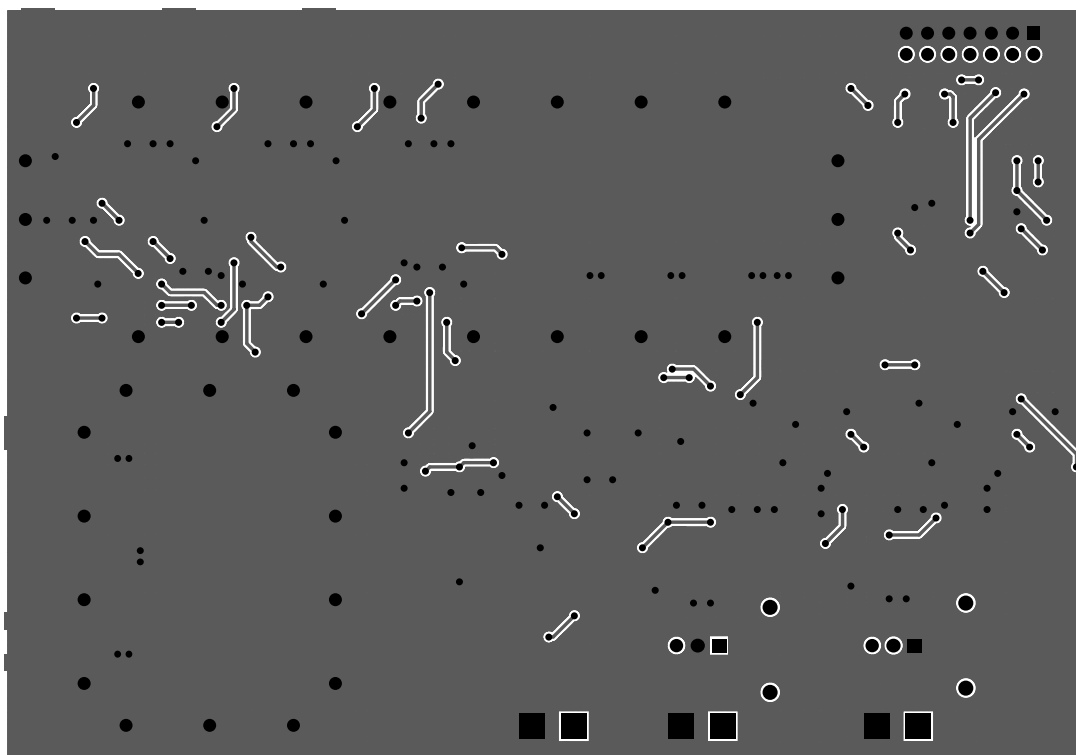


Figure A.1: Full circuit diagram of the Phase Noise Measuring System



(a) Top Layer



(b) Bottom layer

Figure A.2: PCB layouts